UNIVERSITY OF OKLAHOMA

GRADUATE COLLEGE

TEMPERATURE SWING SOLVENT EXTRACTION FOR SELENATE AND SELENITE REMOVAL FROM INDUSTRIAL WASTEWATER

A THESIS

SUBMITTED TO THE GRADUATE FACULTY

in partial fulfillment of the requirements for the

Degree of

MASTER OF SCIENCE

By

MICHAEL S MEISSNER

Norman, Oklahoma

2022

TEMPERATURE SWING SOLVENT EXTRACTION FOR SELENATE AND SELENITE REMOVAL FROM INDUSTRIAL WASTEWATER

A THESIS APPROVED FOR THE

SCHOOL OF CHEMICAL, BIOLOGICAL AND MATERIALS ENGINEERING

BY THE COMMITTEE CONSISTING OF

Dr. Ngoc T. Bui, Chair

Dr. Michele Galizia

Dr. Dimitrios V. Papavassiliou

Acknowledgements

I am grateful to my advisor and committee chair, Dr. Bui, for her unwavering support and guidance. Her insightful comments and patience have encouraged me to think critically about my interests and gain a better understanding of global climate, energy, and water challenges. She has encouraged me to develop new skills and to grow my passion for the act of learning. I am grateful to Dr. Papavassiliou and Dr. Galizia for serving on my committee and the support and knowledge they have provided throughout my time as a graduate student. I am grateful to Andrew D'Amico for his support in building experimental apparatus for research. I am grateful to Dr. Nollert for the support he provided as graduate liaison during my time as a student. I am grateful to all the wonderful people of Dr. Bui's research group.

I would also like to thank Dr. Foster and Alex Frickenstein at the University of Oklahoma Mass Spectrometry, Proteomics, & Metabolomics Core. This work would not have been possible without their assistance in developing an approach to measuring selenium content with inductively coupled plasma mass spectrometry. I am especially grateful to Alex for his time and efforts spent collecting results for my samples with me.

Table of Contents

Abstract

Coal-fired power plants provide more than one fifth of the electricity generated in the United States. Flue gas desulfurization (FGD) of the products of coal combustion is necessary to prevent emissions of SO_2, which is typically accomplished with wet scrubbing systems. The wastewater from these systems contains high levels of gypsum, chloride, and trace heavy elements including selenium. Effective treatment of FGD wastewater remains a challenge. In this thesis, temperature swing solvent extraction was investigated for its ability to produce freshwater from saline and selenium-containing wastewater. Solute rejection for extractions with diisopropylamine (DPA) was dependent on the ionic strength the feed. DPA showed no selectivity for feeds containing 500 ppm selenate and 500 ppm selenite. NaCl rejection of 81% was achieved for a 3.5 w/w% NaCl feed, and the rejection rose to 93% for the 4.0 NaCl feed. For extractions with synthetic FGD wastewater, DPA rejected 86% of feed selenate and 74% of feed NaCl, indicating DPA can treat dilute contaminants in high TDS feeds. Due to the diminishing solute rejection with more dilute feeds, it was concluded that standalone extraction with DPA is not suitable for FGD wastewater treatment. Extraction with decanoic acid displayed over 98% solute rejection for 3.5 w/w%, 1.0 M, and 4.0 M NaCl feeds. Decanoic acid maintained this rejection for feeds containing 500 ppm selenate and 500 ppm selenite, showing stable rejection of ions independent of feed concentrations. The rejection of each species was slightly lower for synthetic FGD wastewater at 96% for selenate and 95% for NaCl. It was concluded that extraction with DA was feasible as a standalone FGD wastewater treatment. Rejections of selenite were higher than selenate, which were higher than chloride. Selenite has the largest hydrated radius and chloride the smallest, suggesting this property influences ion rejection in multicomponent feeds. Finally, higher DA solute rejection but lower water recovery compared to DPA suggests a tradeoff.

Table 1: List of Abbreviations

Abbreviation	Meaning
CFPP	Coal-fired power plant
FGD	Flue gas desulfurization
EPA	Environmental Protection Agency
TSSE	Temperature swing solvent extraction
T_H	Hot step temperature
T_C	Cold step temperature
DPA	Diisopropylamine
DA	Decanoic acid
OA	Octanoic acid
NaCl	Sodium chloride
SeO_4^{2-}	Selenate (from sodium selenate)
SeO_3^{2-}	Selenite (from sodium selenite)
SO_4^{2-}	Sulfate
SO_2	Sulfur dioxide
CO_2	Carbon dioxide
DI	Deionized water
ICP-MS	Inductively Coupled Plasma Mass Spectroscopy

1. Introduction

1.1 Motivation and Significance

Coal-fired power plants (CFPP) are a primary contributor to global electricity production[1]. In 2021, coal accounted for 21.8% of all electricity generated within the United States (US)[2,3]. In CFPPs, coal combustion within coal-fired boilers heats water into steam to generate electricity. The gaseous streams exiting coal-fired boilers in CFPPs are known as flue gas, mainly oxygen (O_2), nitrogen (N_2), carbon dioxide (CO_2), sulfur dioxide (SO_2), and nitrogen oxides (NO_x)[4,5]. CO_2 is the leading cause of climate change[6,7] and a well-known byproduct of coal combustion[6]. Combustion of sulfur deposits in coal feeds release SO_2, a toxic gas and environmental pollutant[8,9] that can cause acid rain[10]. CFPPs implement flue gas desulfurization (FGD) to their gaseous streams before atmospheric release of CO_2 to remove SO_2 from flue gas[11,12]. FGD can be achieved in both wet and dry systems, but wet scrubbing systems are the most widely implemented due to their higher SO_2 removal[12,13]. The standard approach for SO_2 scrubbing is to contact the flue gas with a limestone ($CaCO_3$) slurry to sequester gaseous SO_2 into the slurry as gypsum ($CaSO_4 \cdot 2H_2O$)[14]. Figure 1 shows a schematic of an example FGD wet scrubbing system.

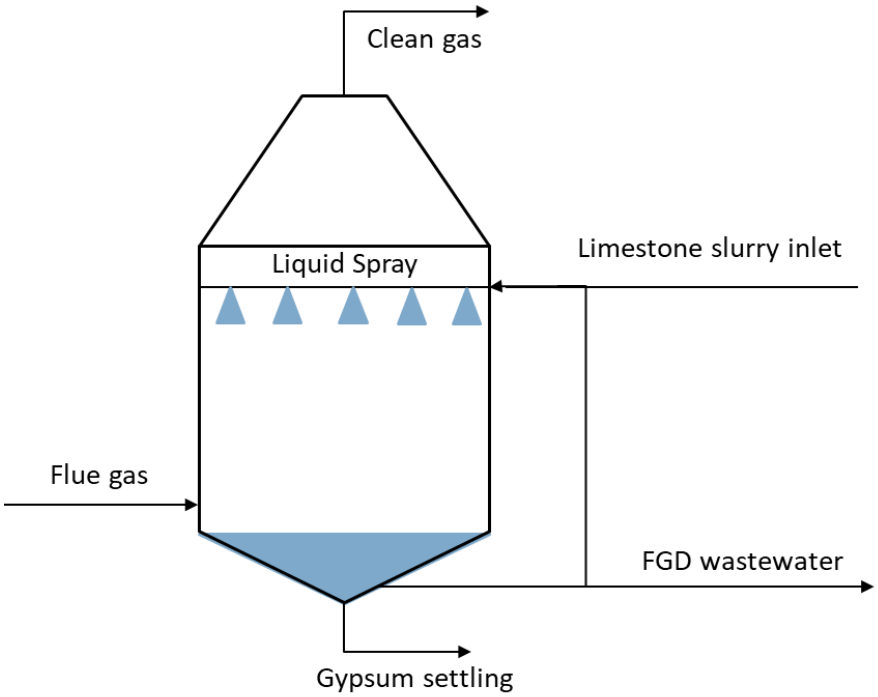

Figure 1: Schematic of an FGD wet scrubbing system. A limestone slurry is sprayed over flue gas to absorb SO_2 from the gas phase into the liquid slurry as $CaSO_4 \cdot 2H_2O$ (gypsum).

There are additional environmentally significant species present in CFPPs. Coal deposits contain several trace elements that were either present at the site of coal formation or that were delivered through groundwater cycles[15,16]. Coal combustion releases these trace elements[17,18], the most notable of which are heavy elements including arsenic, selenium, mercury, and lead[19]. Some of these trace elements partition into FGD wastewaters, including approximately 30% of selenium present in coal feeds[19]. The most common practice for disposing of FGD wastewaters is environmental release after treatment[20], creating significant environmental concern and making coal combustion a major cause of environmental selenium pollution[21–23].

Selenium is an essential trace element to humans and animals, playing a regulatory role in the immune system, thyroid, and reproductive system[24,25]. Selenium deficiencies are associated with impaired immune response[26], arthritis[27], and asthma[28]. However, selenium becomes toxic to

humans above trace levels[29,30]. Symptoms of selenium poisoning include fatigue, hair loss, and gastrointestinal issues[30,31]. Environmental selenium has been linked to high mortality rates in fish and birds[22,32]. Selenium has been shown to bioaccumulate in aquatic systems[33] and can create nonfunctional enzymes via misincorporation into proteins[34].

Selenium exists in several organic and inorganic forms. In water, it exists primarily as the inorganic oxyanions selenate (SeO_4^{2-}) and selenite (SeO_3^{2-}), which are more toxic than the organic and elemental forms[21,35]. Removing selenium oxyanions from wastewater remains a major challenge[22]. The Environmental Protection Agency (EPA) updated effluent limits for environmental discharge of FGD wastewaters until 2015[36], but the technical difficulties involved with compliance to the new FGD wastewater discharge standards caused the EPA to postpone the compliance date for existing CFPPs[37].

Existing methods for selenium removal from FGD effluents include biological reduction and adsorption. Geological variation in coal mines and the rank of coal governs the composition of the FGD wastewater[38]. Biological processes are sensitive to the composition of FGD wastewater[22]. Moreover, biological processes rely on the reduction of SeO_4^{2-} and SeO_3^{2-} into a colloidal, environmentally persistent[39] form of Se^0 instead removal[40,41]. Direct removal processes such as adsorption are limited by the coexistence of sulfate (SO_4^{2-}) ions. Sulfate ions are up to an order of magnitude more prevalent in FGD wastewaters[42] and are structurally similar to selenate ions, which creates competition for adsorption sites[43]. Furthermore, any proposed FGD wastewater treatment must be able to withstand the corrosive and high total dissolved solids (TDS) FGD wastewater. FGD wastewater is recycled through the system to maintain a chloride content of up to 20,000 mg L^{-1}, but chloride contents can reach 40,000 mg L^{-1} with the implementation of corrosion-resistant systems[22,44–46]. A robust process that can withstand variations in FGD

wastewater compositions and remove selenate even in the presence of sulfate and chloride is needed.

Temperature swing solvent extraction (TSSE) is a developing process that could be robust enough to handle the complex and variable nature of FGD wastewater. Section 1.2 will describe the working principles of TSSE. Briefly, TSSE is a cyclical process in which purified water is produced from contaminated feeds. Unlike other solvent extraction processes, the purpose of the solvent is not to transfer the solute between the aqueous and organic phases. Rather, water is drawn from the aqueous phase into the organic, concentrating the feed in a manner comparable to forward osmosis[47] or membrane distillation[48]. The organic and aqueous phases are separated, then a "temperature-swing" of the organic phase shifts the solubility of water and causes a new, purified aqueous layer to form.

1.2 Working Principles of TSSE

In TSSE, contaminated feed water is brought into contact with an organic solvent. The phases reach equilibrium at a temperature where water has a relatively high solubility in the organic phase. As the phases approach equilibrium, the organic phase dissolves water while rejecting feed solutes. The phases are separated, and the organic phase is allowed to reach equilibrium at a different temperature where the solubility of water in the organic phase is low. The water-rich solvent separates into two phases: a water-scarce solvent that can be reused and a new, purified aqueous that can be recovered as product water or subjected to further extractions[49]. Figure 2 outlines the TSSE process.

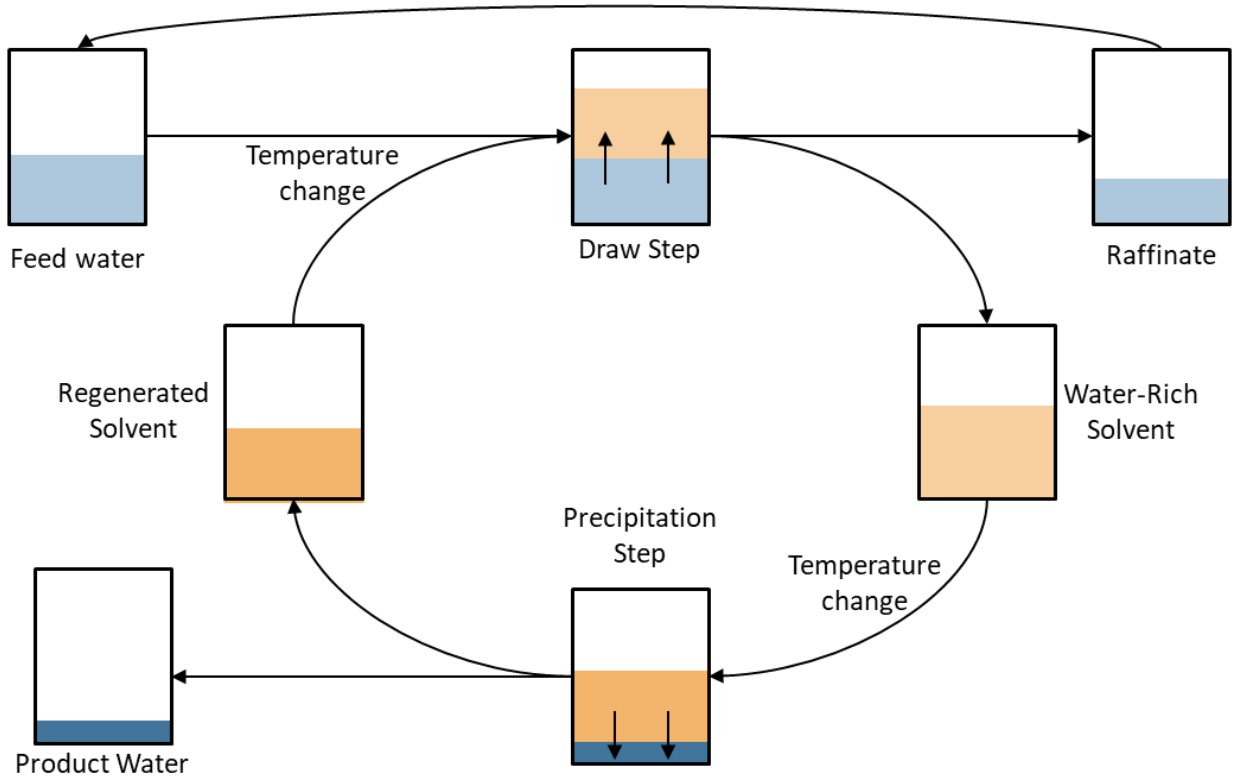

Figure 2: Working diagram of the temperature-swing solvent extraction process. An organic solvent with a polar moiety dissolves water while rejecting solutes within the water. The phases are separated. A "temperature swing" in the organic phase changes water solubility to create a new, purified aqueous phase.

The choice of solvent is the determining factor in process design and performance[50]. Solvents are hydrophobic so that a biphasic system is maintained but contain a hydrophilic moiety that allows the formation of hydrogen bonds with water[51]. Figure 3 shows hydrogen bonding interactions between organic solvents and water.

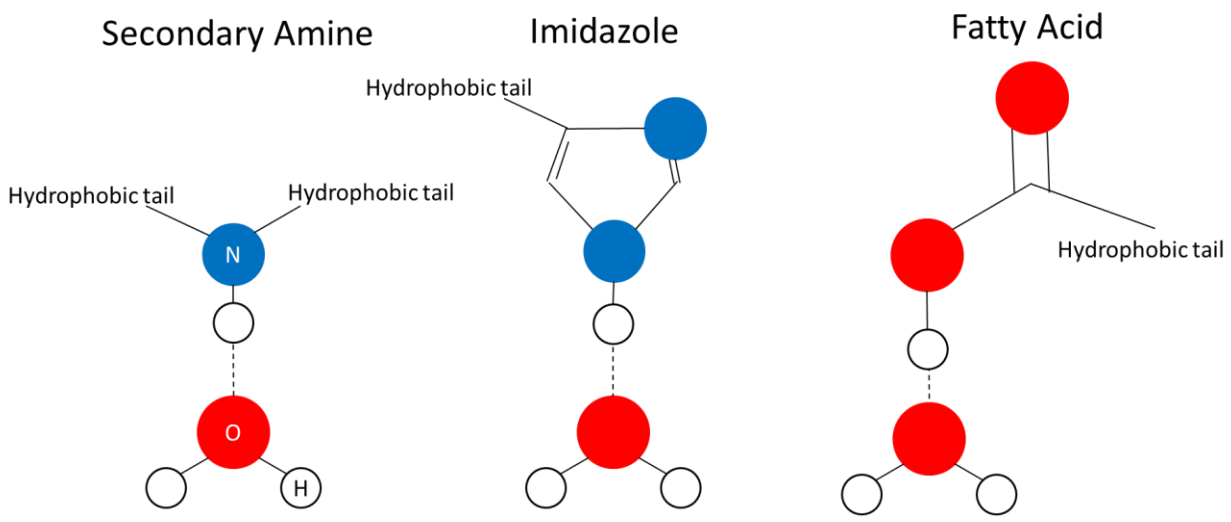

Figure 3: Hydrogen bonding interactions between water and secondary amine, imidazole, and fatty acid organic solvents. Polar portions of the organic solvent form hydrogen bonds with water while hydrophobic tails maintain a biphasic system.

During the first equilibrium step, hereafter referred to as the draw step, the aqueous and organic phases are mixed, then allowed to reach equilibrium at a temperature that promotes hydrogen bonding between molecules of water and solvent, giving water a relatively high solubility in the organic phase. As demonstrated in Figure 3, this equilibrium encourages water to dissolve in the organic phase, while ionic salts remain the polar aqueous layer instead of the hydrophobic solvent[49].

Following the draw step, the phases are separated. The water-rich organic phase is subjected to a second equilibrium phase, hereafter referred to as the precipitation step. During the precipitation step, the solvent is subjected to a temperature that promotes the breaking of the hydrogen bonds between the solvent and water, giving water a relatively low solubility in the organic phase. The breaking of these bonds causes the water to disassociate from the solvent and precipitate into a new aqueous phase[49]. Figure 4 depicts the temperature swing inducing the precipitation step.

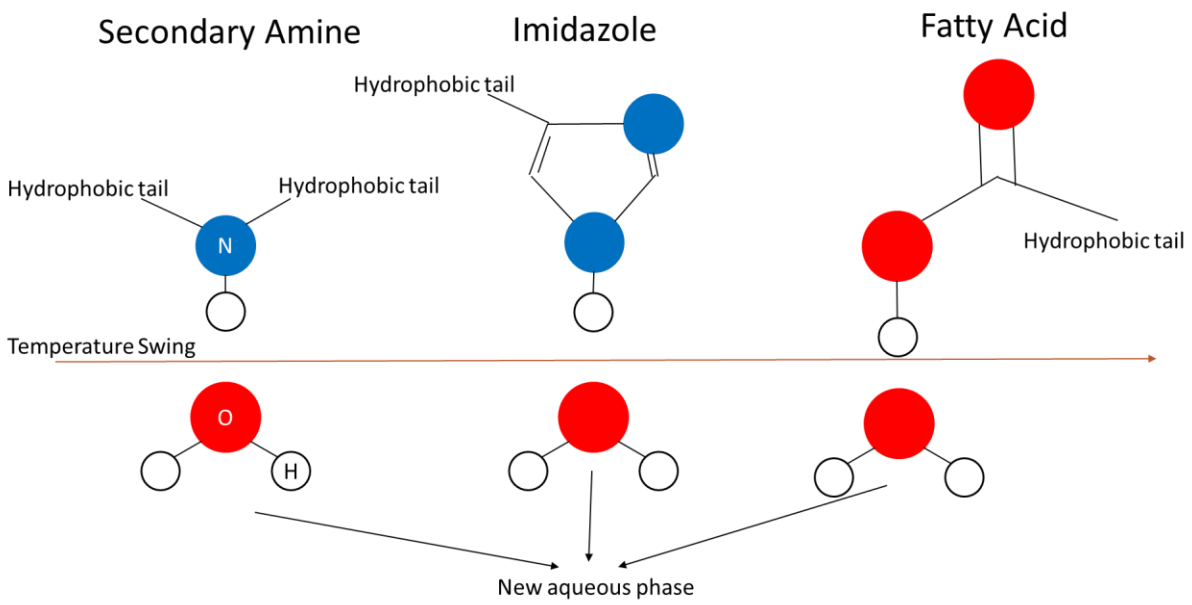

Figure 4: Demonstration of the working principles of TSSE. A temperature swing lowers the solubility of water in the organic solvent, breaking hydrogen bonds and causing the formation of a purified water phase.

The temperature and duration of the draw and precipitation steps depend on the solvent choice. For solvents where dissolving water is exothermic, the draw step is performed at a lower temperature to encourage hydrogen bond formation and the precipitation step is performed at an elevated temperature to break those bonds. For solvents where dissolving water is endothermic, the draw step is performed at an elevated temperature and the precipitation at a lower[52].

Based on these working principles, the ideal solvent for TSSE would have the following properties: It would be sufficiently nonpolar that it forms a biphasic system with water and has negligible miscibility in water; It would be nontoxic such that further treatment of the effluent would not be necessary; It would have polar sites that allow it to absorb significant volumes of water; The solubility of water within the solvent would change dramatically over a small temperature range near ambient temperatures; The solubility of wastewater solutes within the solvent is low; and the solute partition heavily favors the aqueous phase[51,52].

1.3 Commercial Advantage

Although TSSE is not well-studied relative to competing desalination technologies[53–58], it offers several commercial advantages that make it worth exploring. An advantage of TSSE is the potential to integrate heat recovery. Because the solvent is recirculated and undergoes temperature swings, a continuous TSSE process will always have a stream that needs to be heated and one that needs to be cooled. Therefore, the system can be designed with a heat exchanger network for heat recovery. This design improves the thermal efficiency of the process by reducing the total thermal energy demand. Alotaibi *et al* modeled a continuous seawater desalination plant with decanoic acid (DA) and octanoic acid (OA) as the solvent. They find that for OA, the thermal energy consumption ranges from 800 to 900 kWh/^{3} and for DA, it ranges from 1740 to 2300 kWh/m^3 without heat recovery. With heat recovery, the thermal energy consumption for OA has a range of 160 to 180 kWh/m^3. For DA, the thermal energy consumption range is to 350 to 460 kWh/m^3 upon implementation of heat recovery[59]. Figure 5 shows a continuous TSSE process with an optimum heat exchanger network.

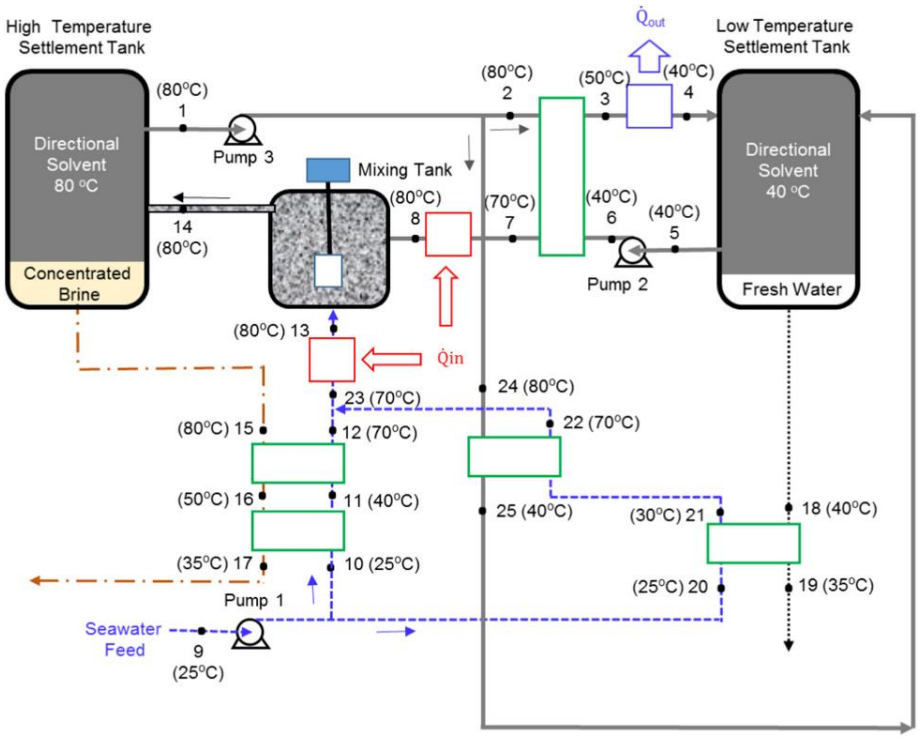

Figure 5: Example of a continuous TSSE process with an optimal heat recovery network. Figure from Alotaibi *et al*[59].

TSSE is a non-evaporative process[51] and has been shown feasible even when the top process temperature is limited to 55 °C[50]. As a result, a TSSE process could be powered by waste or another low-grade source of heat that could be considered inexpensive or free. This gives it a commercial advantage over evaporative or pressure-driven processes when applied in a setting with reliable sources of waste heat such as CFPPs[60].

A common drawback in solvent extraction processes is the need to deploy downstream operations to regenerate solvent before reuse[61,62]. In TSSE, the only necessary solvent regeneration is to precipitate the water, which is already a core step in the process. In principle, the organic solvent will only dissolve water and small amounts of a solute that favors partition into the aqueous phase. Therefore, the precipitation step will remove the water and any solute dissolved within the organic phase, allowing it to be returned directly to the first equilibrium step[49]. The omission of

downstream solvent regeneration reduces the process complexity and eliminates the associated capital and operating expenses. This also minimizes solvent losses and the corresponding organic waste.

Another common drawback to solvent extraction is the environmental and toxicological impacts of the solvents[63,64]. In order to adhere to the principles of green chemistry[65], solvent extraction process development has emphasized the development of ionic liquids applied to solvent extraction processes[66–70]. Ionic liquids are compounds composed of ions but with a melting point below 100 °C. They have low volatilities and are often solid at ambient temperatures, minimizing emissions and secondary pollution concerns. Ionic liquids can be developed to task-specific applications, making them a promising and green alternative to traditional solvents[66,67]. Guo *et al* performed feasibility studies for ionic liquids in TSSE with molecular dynamics simulations and found that 1-ethyl-3-methylimidazolium with an amide anion ([emim][Tf_2N]) was suitable for TSSE, giving an NaCl rejection of 97.5 ± 0.8%[71]. Implementing ionic liquids for TSSE mitigates the volatile organic emission and toxic liquid waste concerns of other solvent extraction processes and would minimize the environmental impacts of TSSE.

A zero liquid discharge (ZLD) process is one that achieves no liquid waste[72]. ZLD processes reduce the volume and environmental impacts of waste, since solid wastes are more readily disposed of in landfills and treated to recover valuable minerals[72,73]. Other ZLD technologies typically involve evaporative systems followed by crystallizers to dewater brines into slurries[74,75]. Boo *et al* have shown that TSSE with diisopropylamine (DPA) can attain ZLD of high salinity brines given a sufficiently high solvent to water ratio. In ZLD TSSE, the water absorbs entirely into the solvent. However, two phases are still present: a single liquid organic phase and

a solid salt precipitate[76]. By separating the liquid solvent and solid precipitate, solid salt and freshwater are recovered with no liquid waste.

The low operating temperatures and temperature swings of TSSE open opportunities for heat recovery networks and waste heat integration. Designs that take advantage of these opportunities reduce the requisite energy input and allow for inexpensive or free waste heat to minimize or eliminate the thermal energy costs of TSSE. The omission of solvent regeneration reduces the cost and complexity of TSSE compared to other solvent extraction processes, and development and adoption of ionic liquids would minimize its environmental impacts. The potential to attain ZLD of brines would further simplify waste handling and reduce its environmental impact. Altogether, these commercial advantages make TSSE a promising desalination process with the potential for minimal environmental impact.

It has been shown that TSSE is capable of achieving high (> 98%) rejections of all major ions in seawater, including Na^+, K^+, Ca^{2+}, Mg^{2+}, Cl^-, and SO_4^{2-}, even in the presence of multiple monovalent and divalent cations[77]. It has also been demonstrated that a single pass of TSSE can achieve removal efficiencies as high as 91% for As-III and 97% for As-V[50]. Experimental and simulated TSSE has primarily included DPA[51,52,76,78,79] and DA[49,50,59,71,77] over a range of ionic solutes. However, no attempt has been made to study TSSE performance for producing freshwater from selenium-containing wastewaters, and comparative studies between DA and DPA have not been performed.

1.4 Hypothesis and Scope

The purpose of this research was to investigate TSSE applied to FGD wastewater and to gain insight into fundamental questions regarding the TSSE process. First, the advantages and tradeoffs of DA and DPA as process solvents were investigated. This information was used to gain insight

onto the existence of a tradeoff between solute rejection and water recovery for TSSE, then the influence of structural differences in these solvents on TSSE performance was considered. The ability of TSSE to reject selenate and selenite was investigated, and the role of the structural differences of these anions on TSSE performance was considered. Selenite, selenate, and chloride rejections are compared to study how differences in ion properties effect solute partition. A mixed system was studied to determine whether individual ion concentration or total feed ionic strength was more influential on process performance. Finally, the results of extraction of a synthetic FGD wastewater sample are considered to judge the feasibility of TSSE in FGD wastewater treatment.

In this study, free energy of solvation simulations were performed for a sodium cation and chloride anion in water, then these results were compared to the free energy of solvation of these species in decanoic acid to determine in which phase dissolved ions would be more stable.

Next, a series of NaCl in water trials were performed at varied NaCl concentrations with DA and DPA as the process solvent. Each feed was extracted three times with the same solvent to validate that no additional regeneration steps were necessary. The NaCl studies are performed to compare the solute rejection and water recovery as a function of concentration for each solvent for saline solutions.

Next, a sodium selenate study and a sodium selenite in aqueous feed study were performed with both process solvents. Finally, extraction of a synthetic FGD wastewater stream containing selenate and NaCl was performed with both solvents. The results are used to discuss the potential of TSSE to treat selenium containing FGD wastewater.

2. Experimental

2.1 Chemicals

Diisopropylamine ($C_6H_{15}N$, ≥99.5%), sodium selenate (Na_2SeO_4, BioXtra), sodium selenite (Na_2SeO_3, 99%), and selenium standard for ICP-MS (1 mg/L Se in nitric acid) were purchased from MilliporeSigma. Sodium chloride (NaCl, certified ACS, crystalline) was purchased from Fisher chemical. Deionized water (DI) was collected from a Milli-Q EQ 7000 ultrapure water purification system.

2.2 Preparation of Stock Solutions

TSSE was performed on six different feeds with two different solvents. NaCl only feeds with concentrations 3.5 weight % (w/w%), 1.0 M, and 4.0 M NaCl were extracted. Then, TSSE was performed on a feed of 500 parts per million (ppm) SeO_4^{2-} and a feed of 500 ppm SeO_3^{2-}. Finally, TSSE was performed on a synthetic FGD wastewater stream containing 20 g L^{-1} Cl^- from NaCl and 500 ppm SeO_4^{2-}. Each feed was extracted with DA and DPA.

Stock solutions of each feed were prepared in sufficient volumes such that a single feed solution could provide the samples for all trials. The appropriate amount of solute to achieve the target feed concentration was weighed, then dissolved into 200 mL DI. Stock solutions were stored in sealed containers in a refrigerator to prevent water evaporation any resulting concentration change. The solutions were allowed to reach room temperature before each use. Target and actual compositions of all stock solutions can be found in Table A1 in Appendix A: Tabulated Data.

2.3 Experimental Procedure for Decanoic Acid

The experimental procedure for studies in which DA was the solvent was based on previous work by Guo *et al*[50]. 10 g DA was weighed on a balance. The actual weights for all DA trials can be found in Table A2 in Appendix A: Tabulated Data. Since DA is solid at room temperature, the DA

was transferred into a beaker and heated in an oven at 60 °C until completely melted. 10 mL feed solution at ambient temperature (~24 °C) was added to a glass vial, followed by the addition of the melted DA. The vial was shaken vigorously, then placed into an oil bath at T_H of 80 °C for 24 hours. Following the draw step, the water-rich organic phase, which was the light phase of the solution, was pipetted into a test tube. A thin layer of DA was intentionally not transferred to ensure no feed was drawn into the pipet. The test tube was placed into an oil bath at T_C of 35 °C for 72 hours to allow an aqueous phase to precipitate from the organic. After precipitation, the DA was pipetted back into the original vial and the extraction process was repeated two more times for a total of three extractions per feed. The volume of the product water was determined. Figure 6 shows the procedure with temperatures labeled for DA trials.

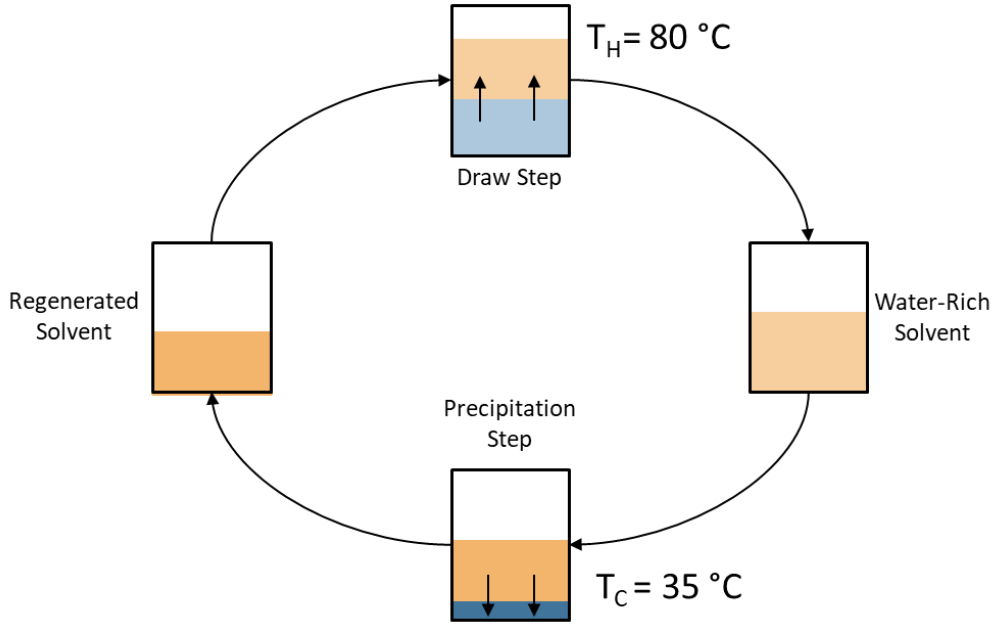

Figure 6: TSSE process for DA. The draw step is performed at 80 °C and the precipitation at 35 °C.

2.4 Experimental Procedure for Diisopropylamine

The experimental procedure for studies in which diisopropylamine (DPA) was the solvent was based on previous work by Boo *et al*[51]. 10 mL feed solution was added to a glass vial with 10 mL DPA. The vials were shaken gently, then placed in an oil bath at T_C of 15 °C for 2h. Next, the water-rich organic phase, which was the light phase of the sample, was carefully pipetted into a separate glass vial. A layer of DPA was intentionally not transferred to avoid drawing feed into the pipet. The new vial was placed in an oil bath at T_H of 65 °C to drive precipitation. After two hours, the DPA was pipetted back into the original vial and the extraction process was repeated two more times for a total of three extractions per feed. The volume of product water was determined. Figure 7 shows the procedure with temperatures labeled for DPA trials.

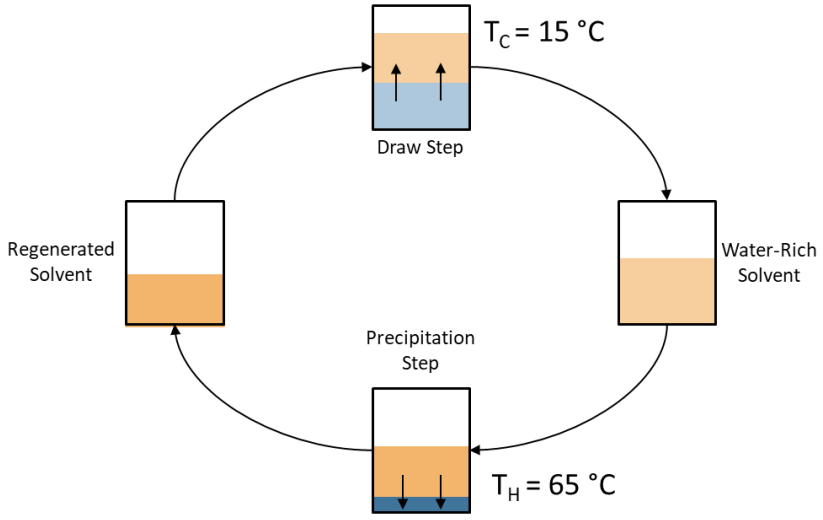

Figure 7: TSSE process for DPA. The draw step is performed at 15 °C and the precipitation at 65 °C.

For DPA and DA extracted samples, chemical analysis of the product water was conducted as soon as possible. When necessary, the product water samples were stored in a sealed container

in the refrigerator. All trials were repeated three times, and the results are reported as mean ± standard deviation.

2.5 Conductivity Measurements

The NaCl concentration of the product water was determined via conductivity measurements with a Thermo scientific Orion Star A212 Conductivity Benchtop Meter. A calibration curve was created with calibration standards.

DPA in the product water created interference in conductivity readings. To ensure reliable NaCl concentration results, an additional calibration curve was generated. To generate the additional calibration curve, 1 mL of standards were brought to equilibrium with DPA at 65 °C, then the standards were diluted to 50 mL with DI to approximate the DPA content of the product water samples.

Samples were diluted to 50 mL with DI before measurement to fully submerge the sensor. The calibration curve was used to calculate the NaCl concentration of the diluted sample, then a mass balance was used to calculate the concentration of the sample before dilution. The pre-dilution concentration was used to calculate solute rejection.

2.6 ICP-MS Measurements

Selenium measurements were conducted with a PerkinElmer NexION2000 Inductively Coupled Plasma Mass Spectrometer (ICP-MS) with Single Cell analysis capability through the University of Oklahoma Mass Spectroscopy, Proteomics, & Metabolomics (MSPM) Core. The system was calibrated with commercial 1 mg/L in 2 w/w% nitric acid selenium standards. Three calibration curves were generated with the commercial standard at 1000 parts per billion (ppb). Additional calibration data was collected with the commercial standard diluted with 2 w/w% nitric acid

solution to 500, 100, 50, and 10 ppb Se. All calibration solutions were spiked with 25 ppb Yttrium as background to ensure consistency between readings.

All readings were conducted under argon, which was ionized at the plasma torch with the introduced experimental samples. Argon forms a dimer, Ar_2, with molar mass 79.2 atomic units (au). This is very similar to the molar mass of Selenium, 78.92 au. For the first calibration curve and SeO_4^{2-} in DA samples, ammonia was introduced in the collision cell in the instrument to remove interferent Ar_2 dimers. In the second calibration curve and the remaining selenate and selenite measurements, helium was introduced in the collision cell instead. The third calibration curve was generated under identical conditions to the second. This calibration curve was used for synthetic FGD wastewater and was generated to ensure accurate readings because the results were collected on a different day. Calibration curves for ICP-MS measurements can be found in Appendix C: Calibration Curves.

All samples were diluted with 2 w/w% nitric acid spiked with 25 ppb Yttrium before ICP-MS analysis. The solutions were diluted to maintain the Se concentration within the calibration curve. For all DPA measurements, 1 microliter of product water was diluted in 3 mL nitric acid solution. DA samples were diluted to an estimated 0.5 ppm Se using the volume of product water recovered and an assumed rejection of 98%. Dilution details for DA ICP-MS measurements can be found in Table A9 in Appendix A: Tabulated Data.

2.7 Simulation Details

Free energy of solvation calculations were performed with Groningen Machine for Chemical Simulation (GROMACS) package version 2021.3 with the coupling factor method[80]. The free energy of solvation for an ion is defined as the free energy change from its configuration in a solid crystalline lattice to its free energy dissolved in solution. There are two distinct steps in this

process: 1) breaking the lattice and 2) dissolution. When comparing the free energy between an ion in different solutions, the first step, breaking the lattice, is unaffected by the choice of solvent. The free energy change of a specific ion after step one but before dissolution into any solution regardless of the liquid is therefore equivalent, and the lattice energy can be excluded from simulations[50,71,80].

When simulating the free energy difference between an ion in two liquids, it is therefore sufficient to calculate the free energy difference from an ion in solution to an ion in a vacuum (i.e., the ion is no longer associated with the crystalline lattice but not yet interacting with the solvent). The free energy difference between the non-interacting and fully interacting states can be calculated by thermodynamic integration with the coupling factor method, shown in Equation 1[80,81].

$$\Delta G = \int_{\lambda_1}^{\lambda_2} \langle \frac{\partial H(\lambda)}{\partial \lambda} \rangle \, d\lambda$$

Equation 1

In this method, the Hamiltonian of the system is adjusted by step changes to the coupling factor λ. At λ = 0, the molecule is fully interacting with the solvent, including Van der Waals and coulombic interactions. At λ = 1, though the ion is still surrounded by solvent in the simulated box, the nonbonding interactions have been turned off and the molecule functionally exists in a vacuum[80,82].

At values $0 < \lambda < 1$, the system is in a nonphysical state in which nonbonding interactions are dampened, slowly decoupling the ion from the solution as λ moves from zero to one. This nonphysical state is governed by "soft core" potentials that depend on λ, shown in Equation 2[82].

$$V_{SC}(r) = (1-\lambda)V^A(r_A) + \lambda V^B(r_B)$$

$$r_A = (\alpha\sigma_A^6\lambda^P + r^6)^{1/6}$$

$$r_B = (\alpha\sigma_B^6(1-\lambda)^P + r^6)^{1/6}$$

Equation 2

where α and p are input parameters and σ is the interaction radius. Equation 2 demonstrates that at λ = 0 and 1, the system is described by the physical, "hard-core" potentials at states A and B. At intermediate states, the "soft-core" potential describes the system[82].

Simulations are performed for a list of lambdas, then trapezoidal numerical thermodynamic integration is performed to estimate the free energy released at each step as the solute is decoupled from the system. The free energy of solvation is the opposite of this value[80–82]. The errors are computed by block averaging. The built-in GROMACS function *bar* computes the free energy and error using the simulation output *.xvg* files[83].

Sodium and chloride ions were modeled with the all-atom optimized potential for liquid simulation (OPLS-aa) model[84]. Water was simulated by the extended simple point charge (SPC/E) model[85]. Decanoic acid was modeled using the GROMOS54A7[86] forcefield and *.itp* and *.pdb* files provided by Automated Topology Builder and Repository[87]. Selenium parameters are not available in any GROMACS forcefields. To simulate selenate, a sulfate molecule was taken from CHARMM-GUI small molecule database[88–90] due to its structural similarity to selenate[43]. The bond lengths of sulfate were scaled by 1.1 to approximate a selenate anion[91,92]. The approximated selenate molecule was modeled with the GROMOS96 forcefield[93,94].

In each simulation, the system first underwent steepest descents minimization. The system was equilibrated at constant volume (NVT ensemble) for 100 ps. A second equilibration was performed at constant pressure (NPT ensemble) for 100 ps. Finally, the production MD run under the NPT ensemble was performed over 1 ns where $\partial H/\partial\lambda$ data was collected and time averaged.

Long range interactions were handled by the Fast Particle-Mesh Ewald (PME)[95] method while a cut-off radius was used for short range van der Waals and coulombic forces.

3. Results

3.1 Simulation Results

Free energy of solvation simulations gave a value of -381.54 ± 0.19 kJ/mol for the sodium cation. This value is comparable to Shi *et al*, who report a value of -92.8 kcal/mol (-388.28 kJ/mol)[96]. For the chloride anion, a value of -370.54 ± 3.06 kJ/mol was obtained. This agrees with the value of -89.22 ± 3.12 kcal/mol (-373.30 ± 13.05 kJ/mol) reported by Smith *et al*[97].

A sodium and chloride ion in DA were simulated by Rish *et al*[77]. They obtain a value of approximately -300 kJ/mol for sodium in DA and -270 kJ/mol for chloride. Figure 8 shows the free energy of sodium and chloride ions in water and DA.

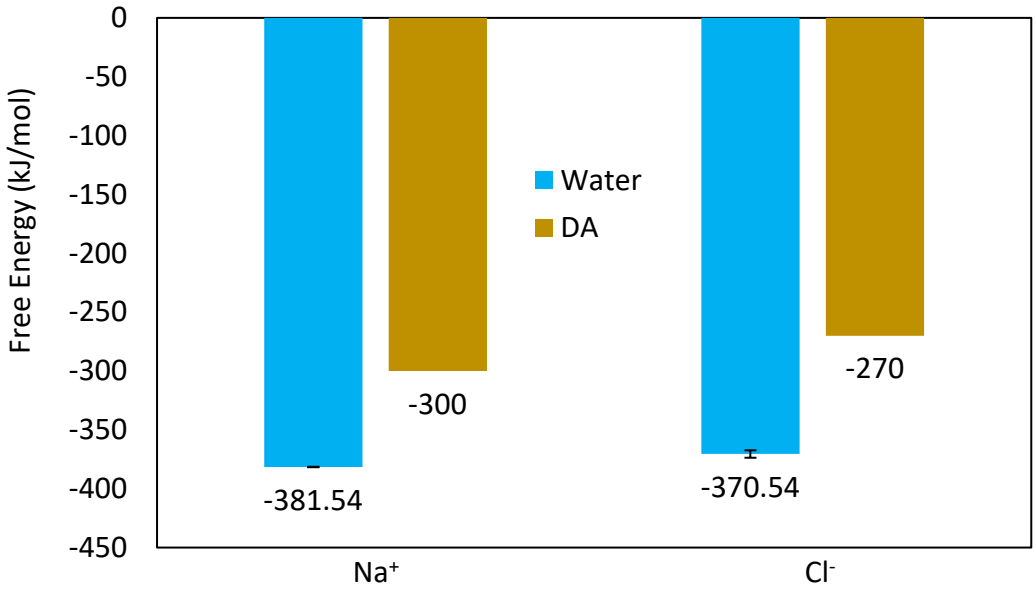

Figure 8: Free energy of solvation of a sodium cation and chloride anion in water and DA.

Systems favor states that minimize the system's Gibbs free energy[98]. As the free energy values demonstrate, an ion in water is more favorable than an ion in solvent. Therefore, it is expected that when DA and water are brought into contact, the solute will favor the aqueous phase and the water recovered from the organic phase will have a lower concentration of solute compared to the feed. This simulation predicts that freshwater will be recovered from TSSE with DA.

3.2 Solvent Recycling

Three cycles of extractions of feeds containing 3.5 w/w%, 1.0 M, and 4.0 M NaCl were performed with DA and DPA. To clarify, an extraction was performed on the feed with an unused solvent. After the precipitation step, the regenerated solvent was used to extract the original feed two more times for a total of three extractions per feed and two reuses of solvent. Figure 9 shows the salinity of the original feed and product water over three extractions with DPA and DA.

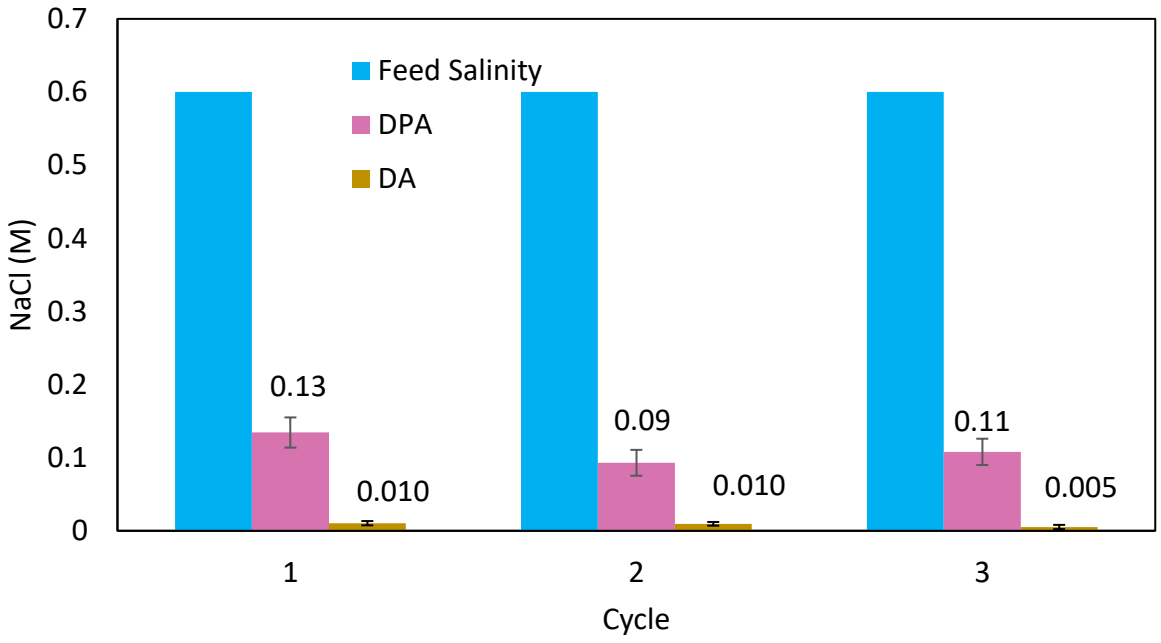

Figure 9: Feed and product water salinity for three cycles of TSSE with 3.5 w/w% NaCl feed and DPA or DA solvent.

As shown in Figure 9, cyclic extraction of the 3.5 w/w% NaCl feed with DA reduced the salinity from 0.6 M to 0.010 ± 0.003, 0.010 ± 0.003, and 0.005 ± 0.003 M NaCl for the first, second, and third cycle, respectively. For extraction of the 3.5 w/w% NaCl feed with DPA, the product water salinity was 0.13 ± 0.02, 0.09 ± 0.02, and 0.11 ± 0.02 M NaCl for the respective cycles.

Figures B1 and B2 in Appendix B: Additional NaCl TSSE Figures show the salinity of the feed and product water for the 1.0 M NaCl feed for DA and DPA extraction, respectively. For 1.0 M NaCl, sequential extraction with DA reduced the product water salinity to 0.018 ± 0.012, 0.018 ± .003, and 0.014 ± 0.015 M NaCl, respectively. For DPA, sequential extraction of the 1.0 M NaCl feed reduced the product salinity to 0.13 ± 0.03, 0.14 ± 0.01, and 0.17 ± 0.01 M NaCl, respectively.

Figures B3 and B4 in Appendix B show the feed and product water salinity over three extractions of 4.0 M NaCl with DA and DPA, respectively. For DA, the product water salinity for three cycles of TSSE was 0.044 ± 0.003, 0.028 ± 0.009, and 0.049 ± 0.021 M NaCl, respectively. For DPA, the product water salinity for the three cycles was 0.18 ± 0.24, 0.26 ± 0.06, and 0.31 ± 0.16 M NaCl, respectively.

For both DA and DPA extraction of all three feeds, the salinity of the product water remains comparable across all three cycles of TSSE. For four of the six runs, all three cycles are similar within error. The only trials that do not agree within error are the first and second cycle for 4.0 M NaCl with DA and the second and third cycle of 1.0 M NaCl extraction with DPA. In the case of 4.0 M NaCl with DA extraction, the third cycle agrees within error of the first and second. In the case of 1.0 M NaCl with DPA extraction, the first cycle agrees within error of the second and third. Therefore, even though not all individual trials agree for these two cases, they do not conflict with

the overall trend that the salinity of the product water remains constant across multiple reuses of solvent.

These results experimentally confirm that for TSSE, the only solvent regeneration necessary is the water precipitation step, which is already a core step in the cycle. The advantage of needing no additional solvent regeneration processes was discussed in Section 1.3.

Cycling the solvent through the process without additional regeneration steps or a solvent purge stream minimizes the liquid waste. However, organic solvents would still need to be replenished due to losses by two mechanisms. The first is solvent partition into the aqueous phase. Bajpayee *et al* report a DA content in the TSSE product water of 36 ppm[49]. Boo *et al* report a DPA concentration of approximately 0.25 M in the product water[76]. Solvent partition into the product water poses two challenges. The first is that solvent that partitions into the product water is solvent that is lost from the cycle and must be replaced. The second is the limitations to the product water applications with organic solutes. DA and DPA are toxic to aquatic ecosystems, and DPA is not readily biodegradable[99,100]. For environmental discharge, effluent toxicity concerns may require additional processes to remove organic compounds. These additional steps increase process complexity and principal and operating costs, which diminishes the commercial viability of TSSE. These environmental concerns suggest that further TSSE development should emphasize identifying or synthesizing solvents with a lower water solubility and that are minimally toxic to aquatic ecosystems.

The second mechanism by which solvent escapes the system is through evaporation. DPA has a boiling point of 84 °C[99], which is only 19 °C above the top process temperature of 65 °C. Volatile organic compound emissions are major sources of air pollution, contributing directly to air quality degradation through the innate toxicity of the volatile substances and indirectly by

acting as ozone and smog precursors[101–105]. The environmental impact of implementing TSSE with volatile solvents means that existing or novel solvents with low volatilities are preferred.

Although both solvents were demonstrated to be recyclable with no solvent regeneration steps, less DA partitions into the product water than DPA, DA is readily environmentally biodegradable[100] and DPA is not, and DA is less volatile (boiling point = 268 °C[100]) than DPA. Therefore, TSSE with DA produces water with lower organic content, lower solvent losses, and lower environmental concerns than DPA.

3.3 Salinity Reduction

Figure 10 shows the average salinity of the product water versus the feed concentration for DA and DPA extractions.

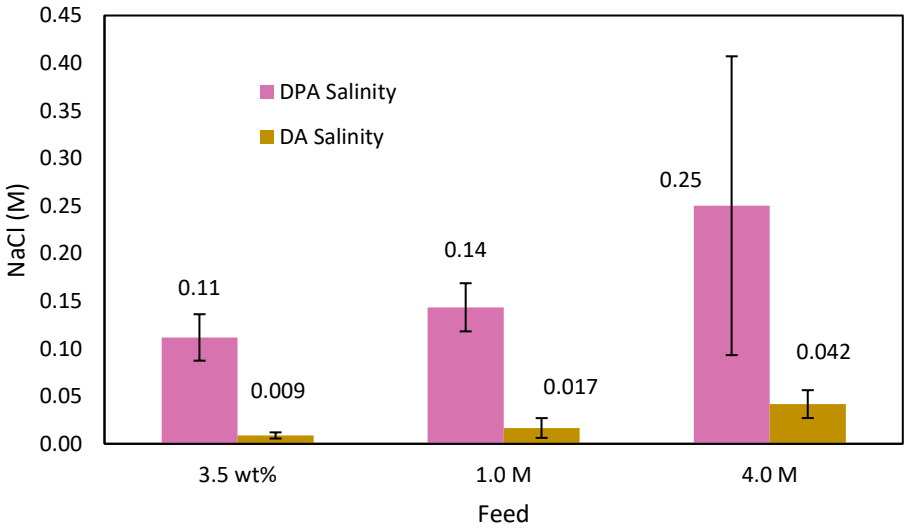

Figure 10: Average product water salinity vs feed concentration for TSSE with DPA and DA.

The product water salinity for DA extractions of 3.5 w/w%, 1.0 M, and 4.0 M NaCl feeds was 0.009 ± 0.003, 0.017 ± 0.010, and 0.042 ± 0.015 M NaCl, respectively. The product water

salinity for DPA extractions of the same feeds was 0.11 ± 0.02, 0.14 ± 0.03, and 0.25 ± 0.16 M NaCl, respectively.

For all three feeds, the product water salinity of the water extracted with DA is approximately an order of magnitude lower than the salinity of the water extracted with DPA. In terms of both solvent partition into the product water and product water salinity, DA extraction produces higher quality water than DPA.

As the salinity of the feed rises, the salinity of the product water rises. For both solvents, the product water produced from the 4.0 M feed has the highest salinity, followed by that from the 1.0 M feed, then the 3.5 w/w% feed. This trend is because TSSE is an equilibrium process in which the solute partitions between the organic and aqueous phase. As the solute concentration in the feed rises, it will also rise in the product water. This trend demonstrates that for applications in which low product water solute concentrations are necessary, the product water from the first cycle of TSSE may need further extraction. This can be achieved by using the effluent from one pass of TSSE as the feed in an additional extraction cycle.

Figure 11 shows the average NaCl rejection across all cycles and NaCl feeds for DPA and DA.

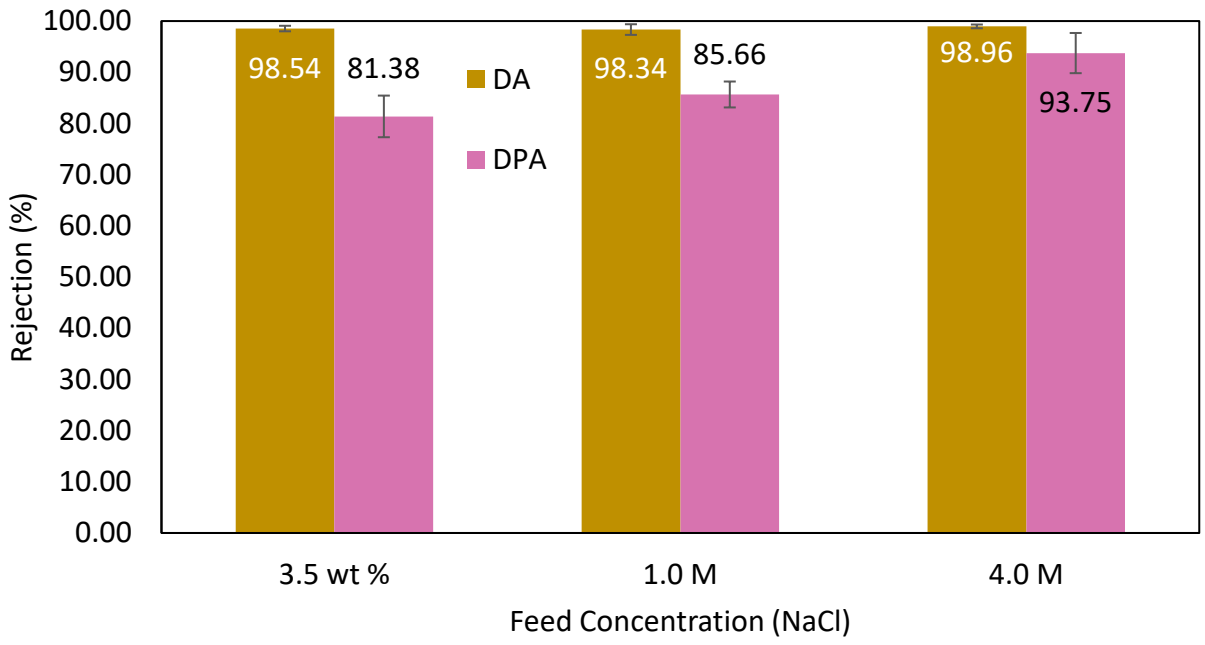

Figure 11: TSSE average salt rejection vs feed concentration for 3.5 w/w%, 1.0 M, and 4.0 M NaCl feeds with DPA solvent.

The NaCl rejection for the 3.5 w/w%, 1.0 M, and 4.0 M NaCl feed after TSSE with DA was 98.54 ± 0.54, 98.34 ± 1.04, and 98.96 ± 0.37%, respectively. The NaCl rejection for these feeds after DPA extraction was 81.38 ± 4.07, 85.66 ± 2.53, and 93.75 ± 3.93%, respectively.

In TSSE with DA, the solute rejection remained consistent regardless of the feed concentration. This agrees with the findings by Rish *et al*, who found that DA solute rejection was relatively constant at ~98% over a span of ions including Na^+, Mg^{2+}, Ca^{2+}, Cl^-, and SO_4^{2-} for feed solute concentrations ranging from 1 to 10.5 wt %[77]. In TSSE trials with DPA, the solute rejection depended on the feed concentration. As the feed concentration increased, the rejection increased. This agrees with the findings by Boo *et al*, who found that the salt removal improved from 86.4% to 95% as the feed concentration increased from 1.0 M to 4.0 M.

These results show that the solute rejection of DA extraction remains constant for desalination of feeds spanning from highly saline brines to the lower ion concentrations of seawater. If this trend holds, then similar rejection rates are expected at the relatively dilute 500 ppm selenate and selenite feeds. The constant rejection rate is advantageous. First, it suggests that TSSE with DA may be capable of treating even dilute feed solutes, such as trace elements in FGD wastewater. Second, it simplifies scale-up designs of TSSE processes. The product water quality is predictable regardless of the initial concentration, so the number of extractions necessary to meet the desired effluent concentration is predictable.

The results for DPA show that rejection depends on the feed concentration. DPA extraction achieves high rejections at 4.0 M NaCl feeds but shows diminishing rejection with decreasing feed concentrations. Achieving very low solute concentrations in the effluent will require several extractions, and each will become less effective as the solute concentration decreases. Additionally, this trend suggests that there might exist a lower bound of solute concentration, below which most selectivity is lost and TSSE with DPA is not a suitable treatment for the feed. Therefore, the selectivity against 500 ppm selenate and selenite feeds is expected to be lower than what was observed for 3.5 w/w% NaCl.

3.4 Selenium Rejection

Three extraction cycles for feeds of 500 ppm as SeO_4^{2-} and SeO_3^{2-} were performed with each solvent. Figure 12 shows feed and product selenate content by cycle for extractions with DA and DPA.

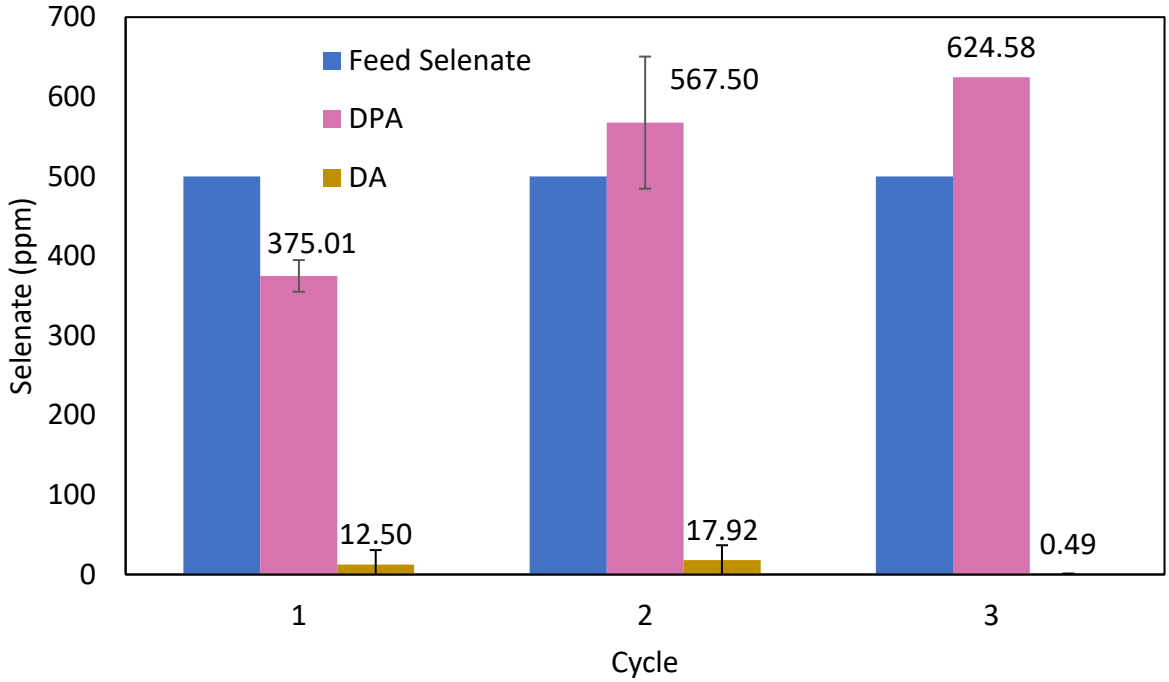

Figure 12: Feed and product water selenate concentration for three cycles of TSSE with 500 ppm SeO_4^{2-} feed and DPA solvent.

The selenate concentration in the product water for three sequential extractions with DA was 12.5 ± 18.2, 17.9 ± 18.8, and 0.5 ± 0.7 ppm as SeO_4^{2-}, respectively. The selenate concentration in the product water for DPA extractions was 375 ± 20, 568 ± 83, and 625 (no standard deviation, only one successful sample) ppm, respectively.

Figure 13 shows feed and product water selenite content by cycle for extractions with DA and DPA.

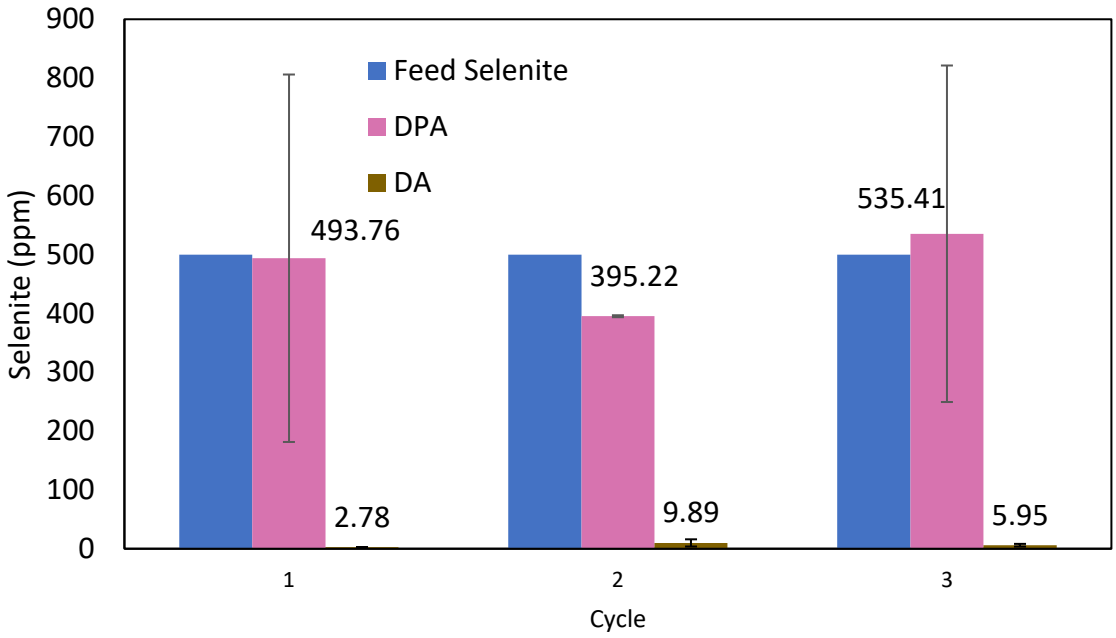

Figure 13: Feed and product water selenite concentration for three cycles of TSSE with 500 ppm SeO_3^{2-} feed and DPA solvent.

The selenite concentration in the product water for DA extractions was 2.78 ± 0.16, 9.89 ± 6.13, and 5.95 ± 2.18 ppm, respectively. The selenite concentration for DPA extracted product water was 493 ± 312, 395 ± 2, and 535 ± 286 ppm, respectively.

Figure 14 shows the solute rejection for 500 ppm SeO_4^{2-} and SeO_4^{2-} feeds with DA and DPA extractions.

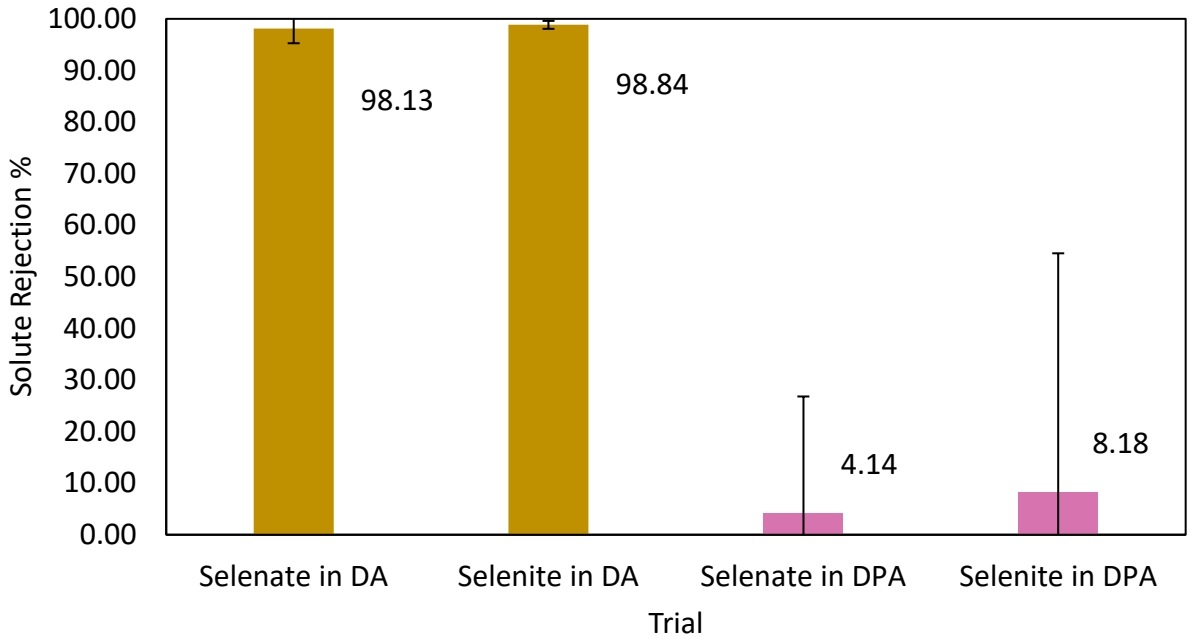

Figure 14: Average TSSE solute rejection for 500 ppm SeO_4^{2-} and SeO_3^{2-} feeds with DA and DPA organic phases.

The selenite rejection after DA extraction was 98.1 ± 2.9%. The selenite rejection with DA extraction was 98.8 ± 0.8%. The selenate rejection with DPA extraction was 4.14 ± 22.66%. The selenite rejection with DPA extraction was 8.18 ± 46.37%.

A single extraction of TSSE with DA reduced the selenate concentration by nearly two orders of magnitude. The selenite concentration in the product water was reduced by a similar degree for selenite feeds extracted with DA. This is consistent with the findings of Guo *et al*, who found that a single pass of TSSE with DA reduced the concentration of arsenite and arsenate by 1-2 orders of magnitude[50]. These results agree with the trend for DA observed in the NaCl trials that DA ion rejection is independent of feed concentration. The solute rejection remains above 98% for the entire range of tested feeds spanning from 500 ppm to 4.0 M solutes, making it well-suited for applications with trace contaminants. Additionally, the high rejection of selenium oxyanions shows TSSE with DA is capable of treating selenium-containing waters, making it a candidate for

FGD wastewater treatment. Finally, it was found that DA showed higher selectivity against selenite than selenate.

For trials with DPA, the solute rejection for SeO_4^{2-} and SeO_3^{2-} is poor. These follow the trend observed in the previous trials where the selectivity of DPA diminishes as the feed becomes more dilute. For the 500 ppm feeds tested here, DPA displayed little selectivity. These findings show that TSSE with DPA is not suitable for feeds containing only low or trace solute concentrations. Like DA, DPA showed higher selectivity against selenite than selenate.

The primary structural difference that exists between selenate and selenite is the molecular geometry of these species. Selenate has four oxygen and is therefore tetrahedral, whereas selenite only has three and is trigonal pyramidal. These structural differences give the molecules different hydrated radii, or the radius of the ion and its strongly associated water molecules. Figure 15 shows the hydrated radius of a selenite and selenate molecule.

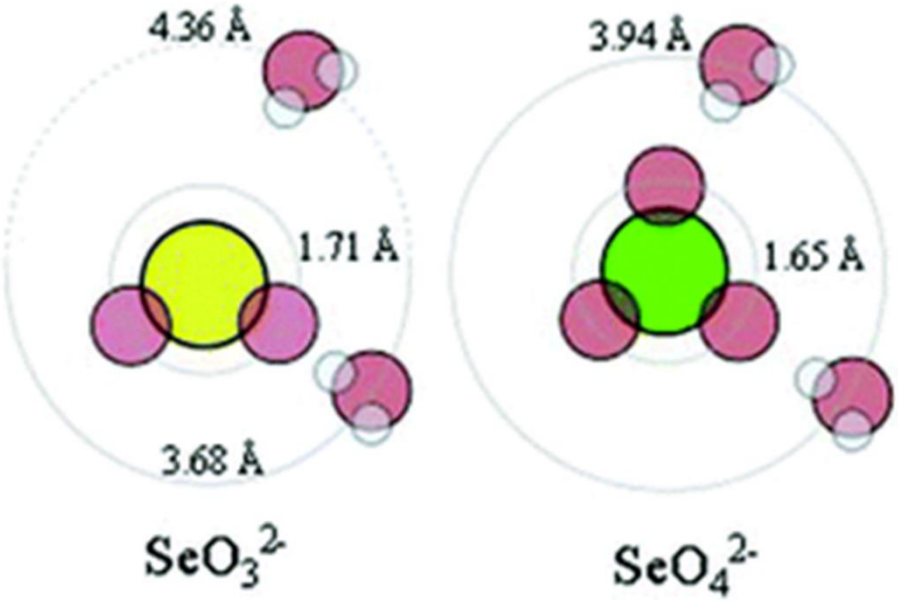

Figure 15: Hydrated radius of selenite and selenate. Figure from Eklund and Persson[92].

In solution, the positive dipole of water molecules form hydrogen bonds with the negative charge of oxygen on the anions. However, on selenite, there is a hemisphere where there is no oxygen with which hydrogen bonds can form. As a result, the hydrated radius is larger for selenite than selenate at 4.36 and 3.94 Å, respectively[92]. A larger hydrated radius may cause the partition to favor the aqueous phase more heavily due to steric considerations. DPA and DA are both bulky molecules, DPA having two isopropyl groups attached to the central amine and DA with a 10-carbon chain. A larger hydrated radius would have more steric interactions with the bulky parts of these molecules that would create an additional barrier to solute partition into the organic phase, resulting in higher rejection for selenite.

3.5 Synthetic FGD Wastewater

Three samples of synthetic FGD wastewater were extracted with DA, and three samples were extracted with DPA. The synthetic FGD wastewater had a chlorine concentration of 20 g/L Cl^- approximate the chloride content of real FGD wastewater[22,44–46] and 500 ppm SeO_4^{2-} to represent the heavy elements. Figure 16 shows feed and product water salinity and selenate content for the synthetic FGD wastewater after extraction with DA and DPA.

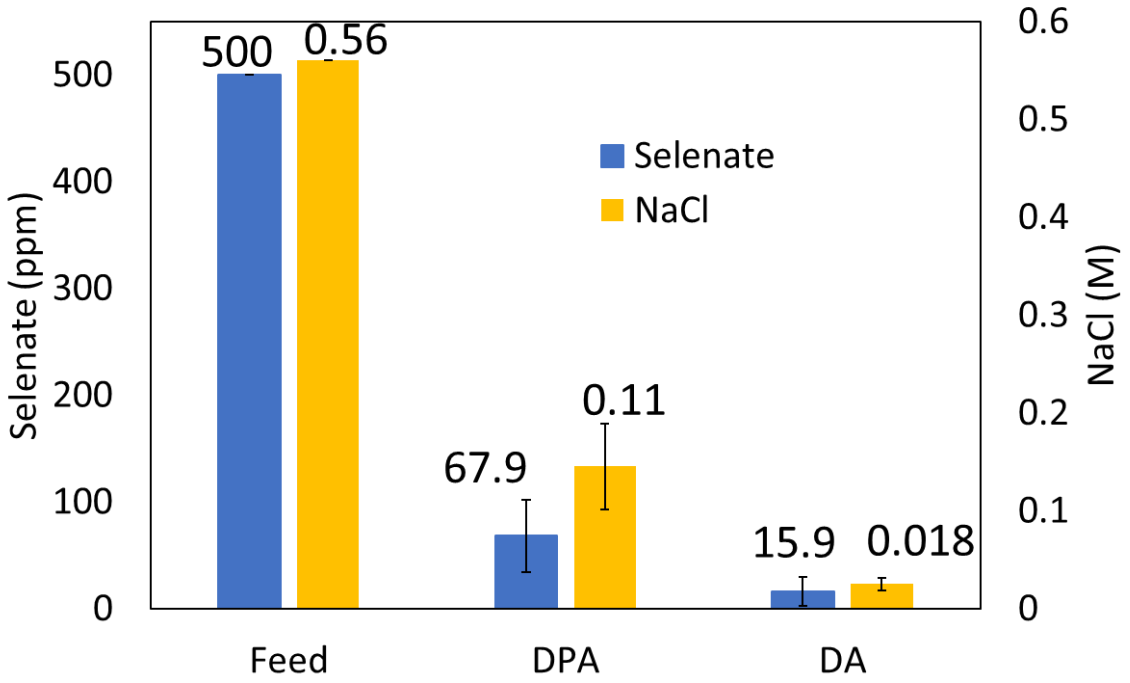

Figure 16: Synthetic FGD wastewater feed and product water salinity and selenate after extraction with DPA and DA.

TSSE of the synthetic FGD wastewater reduced the salinity of the water extracted with DPA to 0.11 ± 0.04 M. The selenate concentration of this product water was 67.9 ± 33.9 ppm. The salinity of the product water for synthetic FGD wastewater extracted with DA was 0.017 ± 0.006 M. The selenate concentration of this water was 15.9 ± 14.0 ppm.

Figure 17 shows the TSSE NaCl and SeO_4^{2} rejection for extraction of synthetic FGD wastewater with DA and DPA.

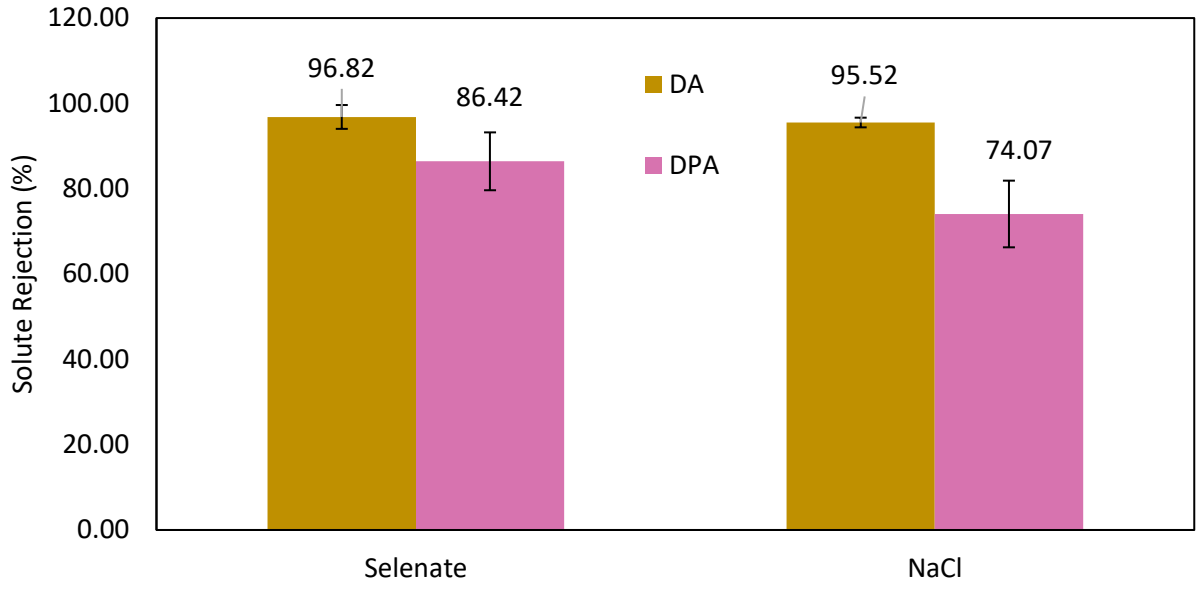

Figure 17: Average TSSE solute rejection for synthetic FGD wastewater feed with DA and DPA organic phases.

The TSSE selenate rejection was 96.82 ± 2.79 and 86.42 ± 6.78% for DA and DPA, respectively. The TSSE NaCl rejection was 95.52 ± 1.14 and 74.07 ± 7.81% for DA and DPA, respectively.

For DPA, the NaCl rejection for synthetic FGD wastewater was lower than it was for 3.5 w/w% NaCl, which was 81.38 ± 4.07%. This agrees with the trend observed for NaCl only feeds, where solute rejection decreased with decreasing feed concentrations. For selenate in the wastewater, DPA showed selectivity. This was not observed with the only solute was 500 ppm selenate or selenite, but selectivity was achieved with the coexistence of relatively concentrated NaCl. This indicates that DPA selectivity depends primarily on the total ionic strength of the feed rather than individual ion concentrations. Selectivity against a low concentration of selenium was achieved, but only when the feed ionic strength was sufficiently high. These results show that DPA

can treat trace contaminants in high TDS feeds. For feeds only containing low levels of solutes, TSSE with DPA is ineffective.

For DA, the rejection of selenate in synthetic FGD wastewater was slightly lower than it was for 500 ppm selenium feeds. The selenium rejection fell from 98.13 ± 2.86% for 500 ppm selenate to 96.82 ± 2.79%. The decrease in both salt and selenate rejection in synthetic FGD wastewater contradicts the findings of the NaCl only and selenium oxyanion only feeds, where the rejection was independent of feed concentration and species. However, a single pass of TSSE with DA achieved more than 95% solute rejection for synthetic FGD wastewater, making it a promising treatment technology for real samples.

For both solvents, a higher rejection was achieved against the selenate anion than NaCl. Since sodium was the only anion in the solution, this shows a higher rejection of selenate with respect to chloride. As mentioned previously, a higher selectivity against selenite was observed than selenate, and now a higher selectivity against selenate is observed than chloride. The hydrated radii of selenite, selenate, and chloride are 4.36, 3.94, and 3.19 Å, respectively[92,106]. This continues the previous trend between hydrated radius and rejection by TSSE. Though this correlation needs further study, it provides insight into how properties of ions influence their partition between phases and resulting rejection by TSSE.

For extraction with DPA, the sodium chloride rejection increased at higher feed concentrations. Virtually no selectivity was observed against 500 ppm selenate alone, but a rejection of 86.42 ± 6.78% was achieved against 500 ppm selenate with the coexistence of sodium chloride at 20 g/L as chloride. This demonstrates that the rejection is dependent on the total ion concentration of the feed rather than the concentration of an individual species. Thermodynamic

modelling explains this observation. Two liquid phases in equilibrium follow the general equilibrium criterion given in Equation 3[98].

$$\bar{f}_i^I(T,P,x^I) = \bar{f}_i^{II}(T,P,x^{II})$$

Equation 3

where f_i^I is the fugacity of species i in phase I, f_i^{II} is the fugacity of species i in phase II, T is the temperature, P is the pressure, and x is the mole fraction of species i in phase I or II. Substituting the activity coefficient definition of fugacity into Equation 3 gives Equation 4.

$$x_i^I \gamma_i^I(T,P,x^I) f_i(T,P) = x_i^{II} \gamma_i^{II}(T,P,x^{II}) f_i(T,P)$$

Equation 4

where γ_i is the activity coefficient of species i in phase I or II and f_i is the pure component liquid fugacity. The pure component liquid fugacity for species i is equivalent on both sides of Equation 4, which is reduced to Equation 5.

$$x_i^I \gamma_i^I(T,P,x^I) = x_i^{II} \gamma_i^{II}(T,P,x^{II})$$

Equation 5

Equations 6 and 7 introduce two terms: the mean ionic activity coefficient and the solution ionic strength. Briefly, these terms approximate the activity or concentration of the ions within a solution rather than considering each individual species.

$$\gamma_{\pm}^{v} = (\gamma_i^*)^{v+}\left(\gamma_j^*\right)^{v-}$$

Equation 6

$$I = \frac{1}{2}\sum_{i=ions} z_i^2 M_i$$

Equation 7

where $\gamma_{\pm}^{v}$ is the mean ionic activity coefficient, $(\gamma_i^*)^{v+}$ represents the activity of the cations, $(\gamma_j^*)^{v-}$ represents the activity of the anions, I is the ionic strength of the solution, z_i is the charge of ion i,

and M_i is the concentration of ion i. With these terms defined, Equation 8 introduces the Debye-Hückel limiting law which relates mean ionic activity to ionic strength.

$$ln(\gamma_{\pm}) = -\alpha|z_+ z_-|\sqrt{I}$$

Equation 8

where α is a parameter that depends on the solvent and temperature. Solving Equation 8 for the mean ionic activity and applying it to Equation 5 gives Equation 9.

$$x_i^I * \exp\left(-\alpha|z_+ z_-|\sqrt{I}\right) = x_i^{II}\gamma_i^{II}(T, P, x^{II})$$

Equation 9

As shown in Equation 9, a higher concentration of salts in the feed will raise I, which will result in the expression within the exponential term having a higher magnitude. As the exponential term is negative, higher ionic strength feeds will cause the mean ionic activity to decrease. On the right side of the equation is the term x_i^{II}, representing the concentration of a given ion in the organic phase. Therefore, for higher ionic strength feeds, less solute will partition into the organic phase and higher rejections will be achieved, which is consistent with the results obtained for DPA. For DA, this is not observed, which means that a different model relating mean ionic activity coefficient to ionic strength is necessary to describe this system.

3.6 Water Recovery

Figure 18 shows the average volume of water recovered per trial for each solvent for each feed. The original volume of all feeds was 10 mL.

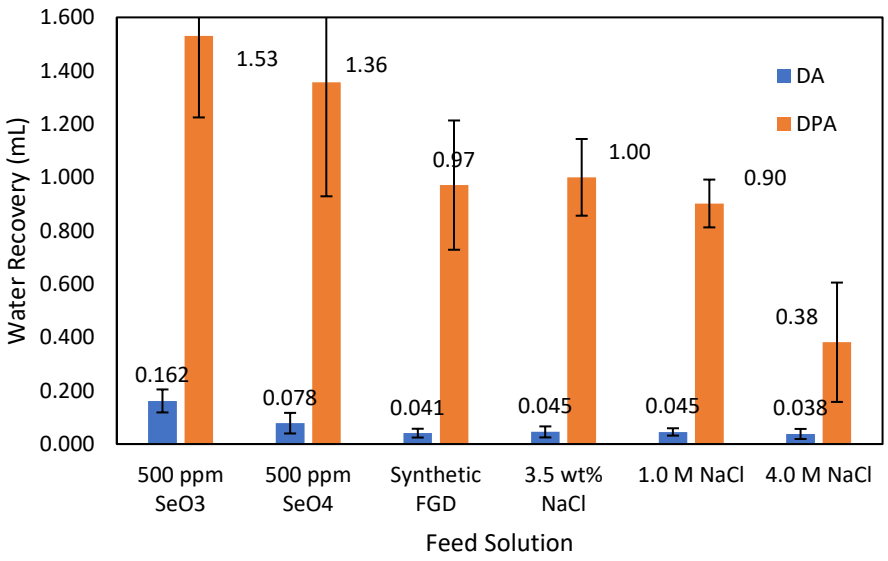

Figure 18: Average water recovery by feed and solvent.

For the SeO_3^{2-}, SeO_4^{2-}, synthetic FGD wastewater, 3.5 w/w% NaCl, 1.0 M NaCl, and 4.0 M NaCl feeds, the water recovery from 10 mL feed extracted with DA was 0.162 ± 0.043, 0.078 ± 0.039, 0.041 ± 0.016, 0.045 ± 0.021, 0.045 ± 0.014, and 0.038 ± 0.019, respectively. For the same feeds with DPA extraction, the water recovery was 1.53 ± 0.31, 1.36 ± 0.43, 0.97 ± 0.24, 1.00 ± 0.14, 0.90 ± 0.09, and 0.38 ± 0.22, respectively.

Figure 18 shows two trends. The first is that water recovery decreases as solute concentration increases. For both DPA and DA, the highest water recovery was achieved for the low solute concentrations of the selenate and selenite feeds. The water recovery decreased as the feed became more concentrated and was lowest for both solvents for the 4.0 M NaCl feed. The second is that DPA achieved 9-22 times higher water recovery than DA, but in every trial, DPA showed worse solute rejection than DA. This suggests that there may exist a tradeoff between water recovery and solute rejection.

The lower water recovery at higher feed concentrations can be explained by thermodynamic modelling. As shown earlier, Equation 5 gives the general equilibrium criteria that applies to each species within each phase.

$$x_i^I \gamma_i^I(T, P, x^I) = x_i^{II} \gamma_i^{II}(T, P, x^{II})$$

Equation 5

Equation 10 gives water activity as a function of solute concentration[98].

$$-ln(\gamma_W) = vmM_W\Phi$$

Equation 10

where γ_w is the water activity coefficient, v is the number of species that form from salt dissolution, m is the molality of solute, M_W is the molar mass of water, and Φ is the osmotic coefficient, which corrects for nonideality. Equation 10 demonstrates that as the concentration of solute within the aqueous phase gets larger, the activity of water gets smaller. Letting phase I be the aqueous phase and phase II the organic, applying Equation 10 to Equation 5 gives Equation 11.

$$x_i^I * \exp(-vmM_W\Phi) = x_i^{II} \gamma_i^{II}(T, P, x^{II})$$

Equation 11

Equation 11 shows that as the solute concentration increases, the left side of the equation decreases. This lowers x_i^{II}, the water concentration in the organic phase. Thus, lower water partition into the organic is expected for more concentrated feeds, so the experimental results agree with thermodynamic modeling.

The second trend was that for all six feeds, the water recovery of DPA was 9-23 times higher than that of DA. A layer of DPA and DA was intentionally not transferred to avoid contaminating the product water, so the high range of DPA/DA water recovery ratios is attributed to variation in the thickness of the remaining layer. Regardless, DPA recovers significantly higher volumes of product water per pass. For TSSE, a higher water recovery raises the process

throughput and lowers the number of cycles necessary to treat a feed, lowering the energy consumption of the process. However, DPA showed a lower solute rejection than DA for all six feeds and gave virtually no rejection for the dilute selenate and selenite feeds. This suggests a tradeoff similar to the selectivity/permeability tradeoff present in membrane separations[107].

However, in the previously mentioned simulations of ionic liquids by Guo *et al* for [emim][Tf_2N], they do not observe this tradeoff. In their work, they report a solute rejection of 97.5 ± 0.8% for [emim][Tf_2N] and a rejection of 96.9-98% for DA. The change in solubility of water per °C temperature change is 0.304 ± 0.023 %/°C for [emim][Tf_2N] compared to 0.025 ± 0.002 %/°C for DA[71]. The greater sensitivity of water solubility to temperature in [emim][Tf_2N] compared to DA suggests that the water recovery would be improved for TSSE with [emim][Tf_2N] with a similar solute rejection to TSSE with DA. If so, this would suggest that solute rejection is primarily dependent on the partition between phases and water recovery is primarily dependent on its solubility shift with temperature, indicating a tradeoff may not exist.

Considering dielectric constants of the phases in the experiments conducted here, on the other hand, shows that a tradeoff between solute rejection and water recovery may be inevitable. The dielectric constant of a species is related to its structure and polarity. For liquids, a high dielectric constant indicates stronger interactions between an ion and the liquid, predicting a higher solubility of ions in that liquid[108,109]. The dielectric constant of DA was estimated based on the constants of other acids[110] to be 2.52, while those of DPA and water are 3.04 and 80.4, respectively. Water has a much higher dielectric constant than DA and DPA, suggesting ion partition will favor the aqueous phase and selectivity will be obtained, which agrees with results for DA at all feed ionic strengths and DPA at high feed ionic strengths. Additionally, DPA has a higher dielectric constant than DA, and a higher rejection is observed for DA.

A quick estimate of the dielectric constant of a mixture of solvents can be performed by adding the product of the mole fraction of each component in the mixture by the dielectric constant of that component[111,112]. Table 2 shows the dielectric constants of the organic and aqueous phases estimated with the mole fraction of each species.

Table 2: Estimated dielectric constants of the aqueous phase, organic phase, and difference for 3.5 w/w% and 4.0M NaCl feed solution in equilibrium with DA or DPA.

System	Organic Phase	Aqueous Phase	Difference
3.5 w/w% in DA	5.7	80.4	74.7
4.0 M in DA	5.8	80.4	74.6
3.5 w/w% in DPA	37.0	80.0	43.0
4.0 M in DPA	20.8	80.0	59.2

Considering the difference in dielectric constants of the aqueous and organic phase describes the experimental results well. First, the difference for 3.5 w/w% and 4.0 M NaCl extracted with DA is 74.7 and 74.6, respectively. These values are quite similar, indicating similar solute rejections should be obtained at both feeds, which was observed. For both feeds, the value of the difference in equilibrium with DA is larger than that for DPA. A larger difference suggests a stronger partition of solute into the aqueous phase, so these values predict a higher solute rejection for extraction by DA than DPA. The experimental results agree with this prediction. Finally, the difference between the aqueous and DPA phase for 3.5 w/w% NaCl is lower than it is for the 4.0 M NaCl feed at 43.0 and 59.2, respectively. This predicts that the solute rejection for the 4.0 M NaCl will be higher than it will for 3.5 w/w% NaCl, which agrees with the experimental results. The differences in dielectric constant difference between the organic and aqueous phases for DA and DPA is due to differences in water recovery.

The water recovery for extraction with DA for the 3.5 w/w% and 4.0 M NaCl feeds was low, at 0.045 ± 0.021and 0.038 ± 0.019 mL, respectively. As a result, the mole fraction of water

within the organic phase remained low and the estimated dielectric constant of the organic phase remained similar to that of DA. Recovery of DPA for these feeds was higher, at 1.00 ± 0.14 and 0.38 ± 0.22 mL, respectively. As a result, the mole fraction of water in the organic phase was higher, especially for the 3.5 w/w% NaCl feed, causing the estimated dielectric constant of the organic phase to increase. These estimates agree well with the experimental results and suggest that a tradeoff between solute rejection and water recovery is inevitable. As the organic phase draws more water, the mole fraction of water in that phase increases. This raises the dielectric constant of the organic phase, lowering the difference between the two phases and causing lower solute rejection. Therefore, any improvements in water recovery may incur a loss in selectivity. The experimental results here suggest a tradeoff may exist, and investigations into a tradeoff represent and excellent opportunity for future research.

4. Discussion

DPA was ineffective at producing freshwater from feeds contaminated with 500 ppm selenate and selenite. For these feeds, the rejections of 4.14 ± 22.66% for selenate and 8.18 ± 46.37% for selenite show that DPA loses its selectivity when the feed solute concentration gets dilute. Accordingly, TSSE with DPA is not suitable for treating dilute feeds. However, the solute rejection for 3.5 w/w%, 1.0 M, and 4.0 M NaCl feeds was 81.38 ± 4.07, 85.66 ± 2.53, and 93.75 ± 3.93%, respectively. For synthetic FGD wastewater, DPA extraction showed selectivity against selenate, giving a rejection of 86.42 ± 6.78%, showing DPA extraction is selective against dilute solutes at higher feed ionic strength. TSSE with DPA is limited in its ability to produce high quality product water, especially when considering the relatively high partition of DPA into the aqueous phase. Therefore, TSSE with DPA is not promising as a standalone treatment for FGD wastewaters. However, DPA TSSE could still be an effective pretreatment for other desalination technologies.

For example, the salinity reduction in a hypersaline feed from a single pass of TSSE could act as a pretreatment for RO, which can be prohibitively energy intensive for feeds with high osmotic pressures[76,113,114].

TSSE with DA showed a high solute rejection independent of the feed concentration. DA showed rejections of over 98% for dilute, 500 ppm selenium oxyanion feeds and those containing 4.0 M NaCl. DA rejection was lower for the synthetic FGD wastewater stream, giving a selenate rejection of 96.82 ± 2.79 and an NaCl rejection of 95.52 ± 1.14. Though these values are slightly lower than the feeds containing only one solute, DA demonstrated high ion rejections that were indiscriminate of the ion species or concentration. TSSE with DA can create freshwater from feeds with salinities approximating what would be encountered in a real FGD wastewater treatment setting. Additionally, it can reject toxic ions of heavy species, including selenium oxyanions shown here and arsenic oxyanions shown by Guo *et al*[50]. Therefore, TSSE with DA solvent is a promising standalone technology for FGD wastewater treatment. However, a major drawback of TSSE with DA is the low water recovery of only 0.41 ± 0.16% of the feed volume for one pass of synthetic FGD wastewater.

Due to the low water recovery, TSSE with DA has a high specific energy consumption of 350 to 460 kWh/m^3 with an optimal heat recovery network[59]. For comparison, reverse osmosis requires 1-7 kWh/m^3, multi-stage flash requires 70-84 kWh/m^3, multiple effect distillation requires 42-67 kWh/m^3, and mechanical vapor compression requires 6.5-12 kWh/m^3 for desalination[115–120]. However, as discussed in section 1.3, this energy could be provided by low grade thermal energy and could therefore be considered free with the integration of waste heat. Membrane distillation is another desalination technology with a relatively high specific energy consumption but that can exploit waste or other low-grade sources of heat to offset the high energy demand. For

FGD wastewater, TSSE has a major advantage over membrane distillation. FGD wastewater is saturated in gypsum ($CaSO_4 \cdot 2H_2O$)[14]. DA TSSE has been shown capable of handling feeds which contain calcium ions and sulfate anions[77]. For membrane distillation, gypsum in the feed water causes mineral scaling, blocking pores and causing a loss of selectivity[121]. Therefore, as long as waste heat integration is implemented, TSSE with DA could be a competitive commercial technology for FGD wastewater, capable of producing fresh water from the saline waste while also removing trace heavy metals.

The low water recovery limits TSSE potential in applications without readily available waste heat. Though the feed can undergo several cycles to raise achieve higher total water recoveries, the low water recovery per cycle causes a high specific energy demand compared to other desalination processes. Solvents with higher water recovery but similar rejection to DA are needed to improve process output without sacrificing selectivity. For an effective solvent, the partition of feed solutes between the organic and aqueous phase would need to strongly favor the aqueous phase. Additionally, the solubility of water within the organic phase would need to have a stronger dependence on temperature than DA.

Although DA is readily biodegradable[100] and has a relatively low concentration of 36 ppm[49] in the product water, the aquatic toxicity of DA poses environmental concern in applications where the effluent will be discharged into the environment. DA shows indiscriminate rejection of ions regardless of species or concentration but could be cost prohibitive because of the low water recovery. DPA gives much higher water recovery than DA, but has lower solute rejection, is volatile, an aquatic hazard[99], and partitions heavily into the product water[76]. Ultimately, broader application of TSSE is limited by faults in the available solvents.

The primary focus of future research should be on identifying and testing new solvents for TSSE. Potential solvents are those that are hydrophobic, creating a biphasic system with water, but contain a moiety that allows hydrogen bonding with water. Potential solvents should be investigated for their suitability as a TSSE solvent. Specifically, solvents in which water solubility has a stronger dependence on temperature will allow for improved water recovery, which will lower the specific energy consumption of the process. Those that achieve high solute rejection regardless of ion or concentration, such as DA, will be more broadly applicable, allowing for remediation of highly saline brines and water contaminated with trace elements with minimal extractions. Finally, solvents that are biodegradable, nonvolatile, and have low miscibility in water should be targeted to maximize the effluent quality and minimize the environmental concerns associated with TSSE. Molecular dynamics simulations are an invaluable tool in estimating the suitability of potential solvents for TSSE. Free energy of solvation calculations can be performed on a solute existing in water and the solvent to estimate which phase the solute will favor[81,82]. Solvents for which solutes strongly favor the aqueous phase are candidates for TSSE. Additional free energy of solvation calculations should be performed for water in solvent and solvent in water to give an indication for the water recovery and solute partition into the effluent. Solvents that are identified as potential TSSE solvents should be experimentally tested. The volatility, aquatic toxicity, and biodegradability should be considered to quantify the environmental impacts of the solvent should be considered to develop selective, green solvents with high throughput for wastewater treatment.

5. Conclusions

Repeated extractions of saline feeds were performed with DA and DPA. For both solvents, the product water quality remained constant despite repeated use of the solvent, demonstrating that

solvent can be recycled directly into the process with no extra regeneration, a major advantage over other solvent extraction processes.

Comparative TSSE studies were performed on DA and DPA, the two leading solvents for this process. DA showed stable NaCl rejections regardless of feed concentration for a 3.5 w/w%, 1.0 M, and 4.0 M NaCl feed. This rejection was maintained for 500 ppm selenate and 500 ppm selenite feeds, showing that DA extraction gives high rejection even for dilute feeds. DPA showed NaCl rejections that depended on the feed concentration, achieving higher rejections for higher feed concentrations. For the dilute selenate and selenite feeds, DPA displayed almost no selectivity against the solutes.

A synthetic FGD wastewater stream with 20 g L^{-1} chloride and 500 ppm was extracted with both solvents. DPA showed a solute rejection of 86.42 ± 6.78% for selenate, against which it had previously shown no selectivity. This means that the total ionic strength of the solution is more important in determining DPA selectivity than the concentration of an individual species. The synthetic FGD stream showed that DPA can treat saline feeds with dilute contaminants but is limited in the quality of product water it can achieve. TSSE with DPA would be suitable as a pretreatment in a TSSE reverse osmosis system, but not as a standalone desalination technology for environmental discharge of FGD wastewater.

DA extraction of the synthetic FGD wastewater achieved solute rejections of 96.82 ± 2.79% for selenate and 95.52 ± 1.14% for NaCl. Though these rejections are lower than the rejections of the NaCl only and selenium oxyanion only feeds, they show that DA can produce high quality water from saline feeds with dilute heavy contaminants. This makes DA feasible as a commercial FGD wastewater treatment technique, but the low water recovery will limit its potential, especially in the absence of waste heat sources.

For the same feed, trials with DPA recovered 9-23 times the volume of water as the trials with DA, though DPA always showed a lower selectivity. This suggests there may be a tradeoff between process productivity and selectivity. However, simulations have identified [emim][Tf_2N] as a suitable solvent for TSSE, giving similar solute rejection to DA but with a stronger water solubility dependence on temperature, indicating higher water recovery with similar rejections is attainable[71]. On the other hand, estimating the dielectric constants of equilibrated systems demonstrated that higher water recovery causes a decline in the dielectric constant difference between the organic and aqueous phases, suggesting that a tradeoff between water recovery and solute rejection is inevitable. The existence of this tradeoff is an opportunity for future research.

Ultimately, TSSE is limited by the range of available solvents. DPA shows low selectivity, partitions strongly into the aqueous product, is volatile, an aquatic hazard, and incapable of treating low TDS feeds. The solubility of water in DA does not shift significantly with temperature, limiting the water recovery per cycle and giving TSSE a high energy consumption. Future TSSE research should use molecular dynamic simulations to identify solvents that will improve process performance. Solvents that water recovery without sacrificing selectivity, especially those that have low miscibility with water, low boiling points, low environmental toxicity, and are biodegradable, are crucial for TSSE to become an economical commercial wastewater treatment process.

5. References

(1) International - U.S. Energy Information Administration (EIA) https://www.eia.gov/international/data/world/coal-and-coke/coal-and-coke-consumption?pd=1&p=0000000000000000000000000000000000000000jg0880000000008&u=0&f=A&v=mapbubble&a=-&i=none&vo=value&&t=C&g=0000000000000000000000000000000000000000000000000001&l=249-ruvvvvvfvtvnvv1vrvvvvfvvvvvvfvvvou20evvvvvvvvvvvnvvvs0008&s=315532800000&e=1577836800000 (accessed 2022 -03 -28).

(2) Frequently Asked Questions (FAQs) - U.S. Energy Information Administration (EIA) https://www.eia.gov/tools/faqs/faq.php (accessed 2022 -03 -28).

(3) Electricity in the U.S. - U.S. Energy Information Administration (EIA) https://www.eia.gov/energyexplained/electricity/electricity-in-the-us.php (accessed 2022 -03 -28).

(4) Bürkle, S.; Becker, L. G.; Dreizler, A.; Wagner, S. Experimental Investigation of the Flue Gas Thermochemical Composition of an Oxy-Fuel Swirl Burner. *Fuel* **2018**, *231*, 61–72. https://doi.org/10.1016/j.fuel.2018.05.039.

(5) Hu, Y.; Naito, S.; Kobayashi, N.; Hasatani, M. CO2, NOx and SO2 Emissions from the Combustion of Coal with High Oxygen Concentration Gases. *Fuel* **2000**, *79* (15), 1925–1932. https://doi.org/10.1016/S0016-2361(00)00047-8.

(6) Feng, K.; Davis, S. J.; Sun, L.; Hubacek, K. Drivers of the US CO2 Emissions 1997–2013. *Nat. Commun.* **2015**, *6* (1), 7714. https://doi.org/10.1038/ncomms8714.

(7) Lacis, A. A.; Schmidt, G. A.; Rind, D.; Ruedy, R. A. Atmospheric CO_2 : Principal Control Knob Governing Earth's Temperature. *Science* **2010**, *330* (6002), 356–359. https://doi.org/10.1126/science.1190653.

(8) Wang, J.; Anthony, E. J. Clean Combustion of Solid Fuels. *Appl. Energy* **2008**, *85* (2–3), 73–79. https://doi.org/10.1016/j.apenergy.2007.07.002.

(9) Pikoñ, K. Environmental Impact of Combustion. *Appl. Energy* **2003**, *75* (3–4), 213–220. https://doi.org/10.1016/S0306-2619(03)00034-5.

(10) Yun, J.; Zhu, C.; Wang, Q.; Hu, Q.; Yang, G. Strong Affinity of Mineral Dusts for Sulfur Dioxide and Catalytic Mechanisms towards Acid Rain Formation. *Catal. Commun.* **2018**, *114*, 79–83. https://doi.org/10.1016/j.catcom.2018.06.011.

(11) Kaminski, J. Technologies and Costs of SO2-Emissions Reduction for the Energy Sector. *Appl. Energy* **2003**, *75* (3–4), 165–172. https://doi.org/10.1016/S0306-2619(03)00029-1.

(12) Srivastava, R. K.; Jozewicz, W. Flue Gas Desulfurization: The State of the Art. *J. Air Waste Manag. Assoc.* **2001**, *51* (12), 1676–1688. https://doi.org/10.1080/10473289.2001.10464387.

(13) U.S. Environmental Protection Agency, Flue Gas Desulfurization - Wet, Spray Dry, and Dry Scrubbers https://www3.epa.gov/ttncatc1/dir1/ffdg.pdf (accessed 2022 -03 -28).

(14) Carletti, C.; Blasio, C. D.; Mäkilä, E.; Salonen, J.; Westerlund, T. Optimization of a Wet Flue Gas Desulfurization Scrubber through Mathematical Modeling of Limestone Dissolution Experiments. *Ind. Eng. Chem. Res.* **2015**, *54* (40), 9783–9797. https://doi.org/10.1021/acs.iecr.5b02691.

(15) Ketris, M. P.; Yudovich, Ya. E. Estimations of Clarkes for Carbonaceous Biolithes: World Averages for Trace Element Contents in Black Shales and Coals. *Int. J. Coal Geol.* **2009**, *78* (2), 135–148. https://doi.org/10.1016/j.coal.2009.01.002.

(16) Vejahati, F.; Xu, Z.; Gupta, R. Trace Elements in Coal: Associations with Coal and Minerals and Their Behavior during Coal Utilization – A Review. *Fuel* **2010**, *89* (4), 904–911. https://doi.org/10.1016/j.fuel.2009.06.013.

(17) Hower, J.; Granite, E.; Mayfield, D.; Lewis, A.; Finkelman, R. Notes on Contributions to the Science of Rare Earth Element Enrichment in Coal and Coal Combustion Byproducts. *Minerals* **2016**, *6* (2), 32. https://doi.org/10.3390/min6020032.

(18) Zhang, Q.; Ghanem, H.; Branam, T. D.; Elswick, E. R.; Olyphant, G. A. Geochemical Characterization of Engineered Coal-Combustion Byproducts (CCBs): Occurrence and Mobility of Trace Elements, Implications for Interactions with Acidic and Ambient Groundwater. *Fuel* **2016**, *177*, 304–314. https://doi.org/10.1016/j.fuel.2016.02.083.

(19) Cheng, C.-M.; Hack, P.; Chu, P.; Chang, Y.-N.; Lin, T.-Y.; Ko, C.-S.; Chiang, P.-H.; He, C.-C.; Lai, Y.-M.; Pan, W.-P. Partitioning of Mercury, Arsenic, Selenium, Boron, and Chloride in a Full-Scale Coal Combustion Process Equipped with Selective Catalytic Reduction, Electrostatic Precipitation, and Flue Gas Desulfurization Systems †. *Energy Fuels* **2009**, *23* (10), 4805–4816. https://doi.org/10.1021/ef900293u.

(20) Technical Development Document for the Effluent Limitations Guidelines and Standards for the Steam Electric Power Generating Point Source Category, 2015.

(21) He, Y.; Xiang, Y.; Zhou, Y.; Yang, Y.; Zhang, J.; Huang, H.; Shang, C.; Luo, L.; Gao, J.; Tang, L. Selenium Contamination, Consequences and Remediation Techniques in Water and Soils: A Review. *Environ. Res.* **2018**, *164*, 288–301. https://doi.org/10.1016/j.envres.2018.02.037.

(22) Gingerich, D. B.; Grol, E.; Mauter, M. S. Fundamental Challenges and Engineering Opportunities in Flue Gas Desulfurization Wastewater Treatment at Coal Fired Power Plants. *Environ. Sci. Water Res. Technol.* **2018**, *4* (7), 909–925. https://doi.org/10.1039/C8EW00264A.

(23) Ohlendorf, H. M.; Covington, S. M.; Byron, E. R.; Arenal, C. A. Conducting Site-Specific Assessments of Selenium Bioaccumulation in Aquatic Systems, 2010.

(24) Hatfield, D. L.; Tsuji, P. A.; Carlson, B. A.; Gladyshev, V. N. Selenium and Selenocysteine: Roles in Cancer, Health, and Development. *Trends Biochem. Sci.* **2014**, *39* (3), 112–120. https://doi.org/10.1016/j.tibs.2013.12.007.

(25) Rotruck, J. T.; Pope, A. L.; Ganther, H. E.; Swanson, A. B.; Hafeman, D. G.; Hoekstra, W. G. Selenium: Biochemical Role as a Component of Glutathione Peroxidase. *Science* **1973**, *179* (4073), 588–590. https://doi.org/10.1126/science.179.4073.588.

(26) Bellinger, F. P.; Raman, A. V.; Reeves, M. A.; Berry, M. J. Regulation and Function of Selenoproteins in Human Disease. *Biochem. J.* **2009**, *422* (1), 11–22. https://doi.org/10.1042/BJ20090219.

(27) Huang, Z.; Rose, A. H.; Hoffmann, P. R. The Role of Selenium in Inflammation and Immunity: From Molecular Mechanisms to Therapeutic Opportunities. *Antioxid. Redox Signal.* **2012**, *16* (7), 705–743. https://doi.org/10.1089/ars.2011.4145.

(28) Schoenmakers, E.; Agostini, M.; Mitchell, C.; Schoenmakers, N.; Papp, L.; Rajanayagam, O.; Padidela, R.; Ceron-Gutierrez, L.; Doffinger, R.; Prevosto, C.; Luan, J.; Montano, S.; Lu, J.; Castanet, M.; Clemons, N.; Groeneveld, M.; Castets, P.; Karbaschi, M.; Aitken, S.; Dixon, A.; Williams, J.; Campi, I.; Blount, M.; Burton, H.; Muntoni, F.; O'Donovan, D.; Dean, A.; Warren, A.; Brierley, C.; Baguley, D.; Guicheney, P.; Fitzgerald, R.; Coles, A.; Gaston, H.; Todd, P.; Holmgren, A.; Khanna, K. K.; Cooke, M.; Semple, R.; Halsall, D.; Wareham, N.; Schwabe, J.; Grasso, L.; Beck-Peccoz, P.; Ogunko, A.; Dattani, M.; Gurnell, M.; Chatterjee, K. Mutations in the Selenocysteine Insertion Sequence–Binding Protein 2 Gene Lead to a Multisystem Selenoprotein Deficiency Disorder in Humans. *J. Clin. Invest.* **2010**, *120* (12), 4220–4235. https://doi.org/10.1172/JCI43653.

(29) Skalnaya, M. G.; Skalny, A. V. ESSENTIAL TRACE ELEMENTS IN HUMAN HEALTH: A PHYSICIAN'S VIEW. *Publ. House Tomsk State Univ.* 224.

(30) Mehri, A. Trace Elements in Human Nutrition (II) - An Update. *Int. J. Prev. Med.* **2020**, *11* (2).

(31) Effects of Selenium and Vitamin E on White Muscle Disease. 2.

(32) Presser, T. S. "The Kesterson Effect." *Environ. Manage.* **1994**, *18* (3), 437–454. https://doi.org/10.1007/BF02393872.

(33) Hamilton, S. J. Review of Selenium Toxicity in the Aquatic Food Chain. *Sci. Total Environ.* **2004**, *326* (1–3), 1–31. https://doi.org/10.1016/j.scitotenv.2004.01.019.

(34) Stadtman, T. C. Selenium Biochemistry: Proteins Containing Selenium Are Essential Components of Certain Bacterial and Mammalian Enzyme Systems. *Science* **1974**, *183* (4128), 915–922. https://doi.org/10.1126/science.183.4128.915.

(35) Mehdi, Y.; Hornick, J.-L.; Istasse, L.; Dufrasne, I. Selenium in the Environment, Metabolism and Involvement in Body Functions. *Molecules* **2013**, *18* (3), 3292–3311. https://doi.org/10.3390/molecules18033292.

(36) Effluent Limitations Guidelines and Standards for Steam Electric Power Generating Point Source Category, 2015.

(37) Postponement of Certain Compliance Dates for the Effluent Limitations Guidelines and Standards for the Steam Electric Power Generating Point Source Category https://www.federalregister.gov/documents/2017/09/18/2017-19821/postponement-of-certain-compliance-dates-for-the-effluent-limitations-guidelines-and-standards-for (accessed 2022 -03 -29).

(38) Treatment Technology Summary For Critical Pollutants of Concern in Power Plant Wastewaters. 88.

(39) Staicu, L. C.; van Hullebusch, E. D.; Lens, P. N. L. Production, Recovery and Reuse of Biogenic Elemental Selenium. *Environ. Chem. Lett.* **2015**, *13* (1), 89–96. https://doi.org/10.1007/s10311-015-0492-8.

(40) Tan, L. C.; Nancharaiah, Y. V.; van Hullebusch, E. D.; Lens, P. N. L. Selenium: Environmental Significance, Pollution, and Biological Treatment Technologies. *Biotechnol. Adv.* **2016**, *34* (5), 886–907. https://doi.org/10.1016/j.biotechadv.2016.05.005.

(41) Staicu, L. C.; Ackerson, C. J.; Cornelis, P.; Ye, L.; Berendsen, R. L.; Hunter, W. J.; Noblitt, S. D.; Henry, C. S.; Cappa, J. J.; Montenieri, R. L.; Wong, A. O.; Musilova, L.; Sura-de Jong, M.; van Hullebusch, E. D.; Lens, P. N. L.; Reynolds, R. J. B.; Pilon-Smits, E. A. H. *Pseudomonas Moraviensis* Subsp. Stanleyae, a Bacterial Endophyte of Hyperaccumulator *Stanleya Pinnata* , Is Capable of Efficient Selenite Reduction to Elemental Selenium under Aerobic Conditions. *J. Appl. Microbiol.* **2015**, *119* (2), 400–410. https://doi.org/10.1111/jam.12842.

(42) Huang, Y. H.; Peddi, P. K.; Tang, C.; Zeng, H.; Teng, X. Hybrid Zero-Valent Iron Process for Removing Heavy Metals and Nitrate from Flue-Gas-Desulfurization Wastewater. *Sep. Purif. Technol.* **2013**, *118*, 690–698. https://doi.org/10.1016/j.seppur.2013.07.009.

(43) Tokunaga, K.; Takahashi, Y. Effective Removal of Selenite and Selenate Ions from Aqueous Solution by Barite. *Environ. Sci. Technol.* **2017**, *51* (16), 9194–9201. https://doi.org/10.1021/acs.est.7b01219.

(44) *Steam Electric Power Generating Point Source Category: Final Detailed Study Report*; EPA 821-R-09-008; US Environmental Protection Agency, 2009.

(45) Electric Power Research Institute. *Conditions Impacting Treatment of Wet Flue Gas Desulfurization Wastewater*; 3002011388; Palo Aloto, CA, 2007; p 40.

(46) Utility Water Act Group. Comments on EPA's Proposed Effluent Limitations Guidelines and Standards for the Steam Electric Power Generating Point Source Category, 2013.

(47) Li, X.-M.; Zhao, B.; Wang, Z.; Xie, M.; Song, J.; Nghiem, L. D.; He, T.; Yang, C.; Li, C.; Chen, G. Water Reclamation from Shale Gas Drilling Flow-Back Fluid Using a Novel Forward Osmosis–Vacuum Membrane Distillation Hybrid System. *Water Sci. Technol.* **2014**, *69* (5), 1036–1044. https://doi.org/10.2166/wst.2014.003.

(48) Alkhudhiri, A.; Darwish, N.; Hilal, N. Membrane Distillation: A Comprehensive Review. *Desalination* **2012**, *287*, 2–18. https://doi.org/10.1016/j.desal.2011.08.027.

(49) Bajpayee, A.; Luo, T.; Muto, A.; Chen, G. Very Low Temperature Membrane-Free Desalination by Directional Solvent Extraction. **2011**, 4.

(50) Guo, J.; Luo, S.; Liu, Z.; Luo, T. Direct Arsenic Removal from Water Using Non-Membrane, Low-Temperature Directional Solvent Extraction. *J Chem Eng Data* **2020**, 9.

(51) Boo, C.; Winton, R. K.; Conway, K. M.; Yip, N. Y. Membrane-Less and Non-Evaporative Desalination of Hypersaline Brines by Temperature Swing Solvent Extraction. *Environ. Sci. Technol. Lett.* **2019**, *6* (6), 359–364. https://doi.org/10.1021/acs.estlett.9b00182.

(52) Barbosa, G. D.; Bara, J. E.; Weinman, S. T.; Turner, C. H. Molecular Aspects of Temperature Swing Solvent Extraction for Brine Desalination Using Imidazole-Based Solvents. *Chem. Eng. Sci.* **2022**, *247*, 116866. https://doi.org/10.1016/j.ces.2021.116866.

(53) Jiang, S.; Li, Y.; Ladewig, B. P. A Review of Reverse Osmosis Membrane Fouling and Control Strategies. *Sci. Total Environ.* **2017**, *595*, 567–583. https://doi.org/10.1016/j.scitotenv.2017.03.235.

(54) Lee, K. P.; Arnot, T. C.; Mattia, D. A Review of Reverse Osmosis Membrane Materials for Desalination—Development to Date and Future Potential. *J. Membr. Sci.* **2011**, *370* (1–2), 1–22. https://doi.org/10.1016/j.memsci.2010.12.036.

(55) Li, X.; Hasson, D.; Semiat, R.; Shemer, H. Intermediate Concentrate Demineralization Techniques for Enhanced Brackish Water Reverse Osmosis Water Recovery – A Review. *Desalination* **2019**, *466*, 24–35. https://doi.org/10.1016/j.desal.2019.05.004.

(56) Abdel-Karim, A.; Leaper, S.; Skuse, C.; Zaragoza, G.; Gryta, M.; Gorgojo, P. Membrane Cleaning and Pretreatments in Membrane Distillation – a Review. *Chem. Eng. J.* **2021**, *422*, 129696. https://doi.org/10.1016/j.cej.2021.129696.

(57) Ahmed, F. E.; Lalia, B. S.; Hashaikeh, R.; Hilal, N. Alternative Heating Techniques in Membrane Distillation: A Review. *Desalination* **2020**, *496*, 114713. https://doi.org/10.1016/j.desal.2020.114713.

(58) Ashoor, B. B.; Mansour, S.; Giwa, A.; Dufour, V.; Hasan, S. W. Principles and Applications of Direct Contact Membrane Distillation (DCMD): A Comprehensive Review. *Desalination* **2016**, *398*, 222–246. https://doi.org/10.1016/j.desal.2016.07.043.

(59) Alotaibi, S.; Ibrahim, O. M.; Luo, S.; Luo, T. Modeling of a Continuous Water Desalination Process Using Directional Solvent Extraction. *Desalination* **2017**, *420*, 114–124. https://doi.org/10.1016/j.desal.2017.07.004.

(60) Zheng, H.; Zheng, C.; Li, X.; Xu, S.; Liu, S.; Zhang, Y.; Weng, W.; Gao, X. Evaporation and Concentration of Desulfurization Wastewater with Waste Heat from Coal-Fired Power Plants. *Environ. Sci. Pollut. Res.* **2019**, *26* (26), 27494–27504. https://doi.org/10.1007/s11356-019-05297-6.

(61) Rodríguez-Llorente, D.; Cañada-Barcala, A.; Álvarez-Torrellas, S.; Águeda, V. I.; García, J.; Larriba, M. A Review of the Use of Eutectic Solvents, Terpenes and Terpenoids in Liquid–Liquid Extraction Processes. *Processes* **2020**, *8* (10), 1220. https://doi.org/10.3390/pr8101220.

(62) Abdul Hadi, N.; Ng, M. H.; Choo, Y. M.; Hashim, M. A.; Jayakumar, N. S. Performance of Choline-Based Deep Eutectic Solvents in the Extraction of Tocols from Crude Palm Oil. *J. Am. Oil Chem. Soc.* **2015**, *92* (11–12), 1709–1716. https://doi.org/10.1007/s11746-015-2720-6.

(63) An, J.; Trujillo-Rodríguez, M. J.; Pino, V.; Anderson, J. L. Non-Conventional Solvents in Liquid Phase Microextraction and Aqueous Biphasic Systems. *J. Chromatogr. A* **2017**, *1500*, 1–23. https://doi.org/10.1016/j.chroma.2017.04.012.

(64) Pena-Pereira, F.; Lavilla, I.; Bendicho, C. Liquid-Phase Microextraction Techniques within the Framework of Green Chemistry. *TrAC Trends Anal. Chem.* **2010**, *29* (7), 617–628. https://doi.org/10.1016/j.trac.2010.02.016.

(65) Sheldon, R. A. The E Factor 25 Years on: The Rise of Green Chemistry and Sustainability. *Green Chem.* **2017**, *19* (1), 18–43. https://doi.org/10.1039/C6GC02157C.

(66) Lei, Z.; Chen, B.; Koo, Y.-M.; MacFarlane, D. R. Introduction: Ionic Liquids. *Chem. Rev.* **2017**, *117* (10), 6633–6635. https://doi.org/10.1021/acs.chemrev.7b00246.

(67) Ventura, S. P. M.; e Silva, F. A.; Quental, M. V.; Mondal, D.; Freire, M. G.; Coutinho, J. A. P. Ionic-Liquid-Mediated Extraction and Separation Processes for Bioactive Compounds: Past, Present, and Future Trends. *Chem. Rev.* **2017**, *117* (10), 6984–7052. https://doi.org/10.1021/acs.chemrev.6b00550.

(68) Lei, Z.; Dai, C.; Chen, B. Gas Solubility in Ionic Liquids. *Chem. Rev.* **2014**, *114* (2), 1289–1326. https://doi.org/10.1021/cr300497a.

(69) Hallett, J. P.; Welton, T. Room-Temperature Ionic Liquids: Solvents for Synthesis and Catalysis. 2. *Chem. Rev.* **2011**, *111* (5), 3508–3576. https://doi.org/10.1021/cr1003248.

(70) Sarmad, S.; Mikkola, J.-P.; Ji, X. Carbon Dioxide Capture with Ionic Liquids and Deep Eutectic Solvents: A New Generation of Sorbents. *ChemSusChem* **2017**, *10* (2), 324–352. https://doi.org/10.1002/cssc.201600987.

(71) Guo, J.; Tucker, Z. D.; Wang, Y.; Ashfeld, B. L.; Luo, T. Ionic Liquid Enables Highly Efficient Low Temperature Desalination by Directional Solvent Extraction. *Nat. Commun.* **2021**, *12* (1), 437. https://doi.org/10.1038/s41467-020-20706-y.

(72) Tong, T.; Elimelech, M. The Global Rise of Zero Liquid Discharge for Wastewater Management: Drivers, Technologies, and Future Directions. *Environ. Sci. Technol.* **2016**, *50* (13), 6846–6855. https://doi.org/10.1021/acs.est.6b01000.

(73) Guo, J.; Zhou, Z.; Ming, Q.; Sun, D.; Li, F.; Xi, J.; Wu, Q.; Yang, J.; Xia, Q.; Zhao, X. Recovering Chemical Sludge from the Zero Liquid Discharge System of FLue Gas Desulfurization Wastewater as Flame Retardants by a Stepwise Precipitation Process. *J. Hazard. Mater.* **2021**, *417*, 126054. https://doi.org/10.1016/j.jhazmat.2021.126054.

(74) Liang, Y.; Lin, X.; Kong, X.; Duan, Q.; Wang, P.; Mei, X.; Ma, J. Making Waves: Zero Liquid Discharge for Sustainable Industrial Effluent Management. *Water* **2021**, *13* (20), 2852. https://doi.org/10.3390/w13202852.

(75) Morillo, J.; Usero, J.; Rosado, D.; El Bakouri, H.; Riaza, A.; Bernaola, F.-J. Comparative Study of Brine Management Technologies for Desalination Plants. *Desalination* **2014**, *336*, 32–49. https://doi.org/10.1016/j.desal.2013.12.038.

(76) Boo, C.; Billinge, I. H.; Chen, X.; Shah, K. M.; Yip, N. Y. Zero Liquid Discharge of Ultrahigh-Salinity Brines with Temperature Swing Solvent Extraction. *Environ. Sci. Technol.* **2020**, *54* (14), 9124–9131. https://doi.org/10.1021/acs.est.0c02555.

(77) Rish, D.; Luo, S.; Kurtz, B.; Luo, T. Exceptional Ion Rejection Ability of Directional Solvent for Non-Membrane Desalination. *Appl. Phys. Lett.* **2014**, *104* (2), 024102. https://doi.org/10.1063/1.4861835.

(78) Sappidi, P.; Barbosa, G.; Rabideau, B. D.; Weinman, S. T.; Turner, C. H. Molecular Simulation of High-Salinity Brines in Contact with Diisopropylamine and Tripropylamine Solvents. *Ind. Eng. Chem. Res.* **2021**, *60* (21), 7917–7925. https://doi.org/10.1021/acs.iecr.1c01057.

(79) Zhang, H.; Lai, Y.; Yang, X.; Li, C.; Dong, Y. Non-Evaporative Solvent Extraction Technology Applied to Water and Heat Recovery from Low-Temperature Flue Gas: Parametric Analysis and Feasibility Evaluation. *Energy* **2022**, *244*, 123062. https://doi.org/10.1016/j.energy.2021.123062.

(80) Straatsma, T. P.; McCammon, J. A. Computational Alchemy. 29.

(81) Free energy calculations — GROMACS 2022 documentation https://manual.gromacs.org/documentation/current/reference-manual/algorithms/free-energy-calculations.html (accessed 2022 -03 -30).

(82) Free energy interactions — GROMACS 2019.1 documentation https://manual.gromacs.org/2019.1/reference-manual/functions/free-energy-interactions.html#soft-core-interactions (accessed 2022 -03 -30).

(83) GROMACS Documentation.

(84) Jorgensen, W. L.; Maxwell, D. S.; Tirado-Rives, J. Development and Testing of the OPLS All-Atom Force Field on Conformational Energetics and Properties of Organic Liquids. *J. Am. Chem. Soc.* **1996**, *118* (45), 11225–11236. https://doi.org/10.1021/ja9621760.

(85) Berendsen, H. J. C.; Grigera, J. R.; Straatsma, T. P. The Missing Term in Effective Pair Potentials. *J. Phys. Chem.* **1987**, *91* (24), 6269–6271. https://doi.org/10.1021/j100308a038.

(86) Schmid, N.; Eichenberger, A.; Choutko, A.; Riniker, S.; Winger, M.; Mark, A.; van Gunsteren, W. Definition and Testing of the GROMOS Force-Field Versions 54A7 and 54B7. *Eur. Biophys. J.* **2011**, *40*, 843–856.

(87) Koziara, K. B.; Stroet, M.; Malde, A. K.; Mark, A. E. Testing and Validation of the Automated Topology Builder (ATB) Version 2.0: Prediction of Hydration Free Enthalpies. *J. Comput. Aided Mol. Des.* **2014**, *28* (3), 221–233. https://doi.org/10.1007/s10822-014-9713-7.

(88) Brooks, B. R.; Brooks, C. L.; Mackerell, A. D.; Nilsson, L.; Petrella, R. J.; Roux, B.; Won, Y.; Archontis, G.; Bartels, C.; Boresch, S.; Caflisch, A.; Caves, L.; Cui, Q.; Dinner, A. R.; Feig, M.; Fischer, S.; Gao, J.; Hodoscek, M.; Im, W.; Kuczera, K.; Lazaridis, T.; Ma, J.; Ovchinnikov, V.; Paci, E.; Pastor, R. W.; Post, C. B.; Pu, J. Z.; Schaefer, M.; Tidor, B.; Venable, R. M.; Woodcock, H. L.; Wu, X.; Yang, W.; York, D. M.; Karplus, M. CHARMM: The Biomolecular Simulation Program. *J. Comput. Chem.* **2009**, *30* (10), 1545–1614. https://doi.org/10.1002/jcc.21287.

(89) Lee, J.; Cheng, X.; Swails, J. M.; Yeom, M. S.; Eastman, P. K.; Lemkul, J. A.; Wei, S.; Buckner, J.; Jeong, J. C.; Qi, Y.; Jo, S.; Pande, V. S.; Case, D. A.; Brooks, C. L.; MacKerell, A. D.; Klauda, J. B.; Im, W. CHARMM-GUI Input Generator for NAMD, GROMACS, AMBER, OpenMM, and CHARMM/OpenMM Simulations Using the CHARMM36 Additive Force Field. *J. Chem. Theory Comput.* **2016**, *12* (1), 405–413. https://doi.org/10.1021/acs.jctc.5b00935.

(90) Jo, S.; Kim, T.; Iyer, V. G.; Im, W. CHARMM-GUI: A Web-Based Graphical User Interface for CHARMM. *J. Comput. Chem.* **2008**, *29* (11), 1859–1865. https://doi.org/10.1002/jcc.20945.

(91) Louisnathan, S. J.; Hill, R. J.; Gibbs, G. V. Tetrahedral Bond Length Variations in Sulfates. *Phys. Chem. Miner.* **1977**, *1* (1), 53–69. https://doi.org/10.1007/BF00307979.

(92) Eklund, L.; Persson, I. Structure and Hydrogen Bonding of the Hydrated Selenite and Selenate Ions in Aqueous Solution. *Dalton Trans* **2014**, *43* (17), 6315–6321. https://doi.org/10.1039/C3DT53468E.

(93) Scott, W. R. P.; Hünenberger, P. H.; Tironi, I. G.; Mark, A. E.; Billeter, S. R.; Fennen, J.; Torda, A. E.; Huber, T.; Krüger, P.; van Gunsteren, W. F. The GROMOS Biomolecular Simulation Program Package. *J. Phys. Chem. A* **1999**, *103* (19), 3596–3607. https://doi.org/10.1021/jp984217f.

(94) Oostenbrink, C.; Villa, A.; Mark, A. E.; Van Gunsteren, W. F. A Biomolecular Force Field Based on the Free Enthalpy of Hydration and Solvation: The GROMOS Force-Field

Parameter Sets 53A5 and 53A6. *J. Comput. Chem.* **2004**, *25* (13), 1656–1676. https://doi.org/10.1002/jcc.20090.

(95) Darden, T.; York, D.; Pedersen, L. Particle Mesh Ewald: An *N* ·log(*N*) Method for Ewald Sums in Large Systems. *J. Chem. Phys.* **1993**, *98* (12), 10089–10092. https://doi.org/10.1063/1.464397.

(96) Shi, Y.; Beck, T. L. Absolute Ion Hydration Free Energy Scale and the Surface Potential of Water via Quantum Simulation. *Proc. Natl. Acad. Sci.* **2020**, *117* (48), 30151–30158. https://doi.org/10.1073/pnas.2017214117.

(97) Smith, E. J.; Bryk, T.; Haymet, A. D. J. Free Energy of Solvation of Simple Ions: Molecular-Dynamics Study of Solvation of Cl− and Na+ in the Ice/Water Interface. *J. Chem. Phys.* **2005**, *123* (3), 034706. https://doi.org/10.1063/1.1953578.

(98) Sandler, S. I. *Chemical, Biochemical, and Engineering Thermodynamics*, 5th ed.; Wiley, 2017.

(99) Diisopropylamine Safety Data Sheet. *Sigma-Aldrich* **2022**, 11.

(100) Decanoic Acid Safety Data Sheet. *Sigma-Aldrich* **2021**, 9.

(101) Rodhe, H. A Comparison of the Contribution of Various Gases to the Greenhouse Effect. *Science* **1990**, *248* (4960), 1217–1219. https://doi.org/10.1126/science.248.4960.1217.

(102) Peng, J.; Wang, S. Performance and Characterization of Supported Metal Catalysts for Complete Oxidation of Formaldehyde at Low Temperatures. *Appl. Catal. B Environ.* **2007**, *73* (3–4), 282–291. https://doi.org/10.1016/j.apcatb.2006.12.012.

(103) Lakshmanan, P.; Delannoy, L.; Richard, V.; Méthivier, C.; Potvin, C.; Louis, C. Total Oxidation of Propene over Au/XCeO2-Al2O3 Catalysts: Influence of the CeO2 Loading and the Activation Treatment. *Appl. Catal. B Environ.* **2010**, *96* (1–2), 117–125. https://doi.org/10.1016/j.apcatb.2010.02.009.

(104) Amann, M.; Lutz, M. The Revision of the Air Quality Legislation in the European Union Related to Ground-Level Ozoneq. **2000**, 22.

(105) Kamal, M. S.; Razzak, S. A.; Hossain, M. M. Catalytic Oxidation of Volatile Organic Compounds (VOCs) – A Review. *Atmos. Environ.* **2016**, *140*, 117–134. https://doi.org/10.1016/j.atmosenv.2016.05.031.

(106) Marcus, Y. Ionic Radii in Aqueous Solutions. 24.

(107) Wang, W.; Du, X.; Vahabi, H.; Zhao, S.; Yin, Y.; Kota, A. K.; Tong, T. Trade-off in Membrane Distillation with Monolithic Omniphobic Membranes. *Nat. Commun.* **2019**, *10* (1), 3220. https://doi.org/10.1038/s41467-019-11209-6.

(108) Cardona, J.; Jorge, M.; Lue, L. Simple Corrections for the Static Dielectric Constant of Liquid Mixtures from Model Force Fields. *Phys. Chem. Chem. Phys.* **2020**, *22* (38), 21741–21749. https://doi.org/10.1039/D0CP04034G.

(109) Abolghassemi Fakhree, M. A.; Delgado, D. R.; Martínez, F.; Jouyban, A. The Importance of Dielectric Constant for Drug Solubility Prediction in Binary Solvent Mixtures: Electrolytes and Zwitterions in Water + Ethanol. *AAPS PharmSciTech* **2010**, *11* (4), 1726–1729. https://doi.org/10.1208/s12249-010-9552-3.

(110) Phadke, R. S. Studies in the Dielectric Constants of Fatty Acids.

(111) Ascani, M.; Held, C. Prediction of Salting-out in Liquid-Liquid Two-Phase Systems with EPC-SAFT: Effect of the Born Term and of a Concentration-Dependent Dielectric Constant. *J. Inorg. Gen. Chem.* **2021**, No. 647, 1305–1314. https://doi.org/10.1002/zaac.202100032.

(112) Neumaier, L.; Schilling, J.; Bardow, A.; Gross, J. Dielectric Constant of Mixed Solvents Based on Perturbation Theory. *Fluid Phase Equilibria* **2022**, *555*, 113346. https://doi.org/10.1016/j.fluid.2021.113346.

(113) Martinetti, C. R.; Childress, A. E.; Cath, T. Y. High Recovery of Concentrated RO Brines Using Forward Osmosis and Membrane Distillation. *J. Membr. Sci.* **2009**, *331* (1–2), 31–39. https://doi.org/10.1016/j.memsci.2009.01.003.

(114) Shannon, M. A.; Bohn, P. W.; Elimelech, M.; Georgiadis, J. G.; Mariñas, B. J.; Mayes, A. M. Science and Technology for Water Purification in the Coming Decades. *Nature* **2008**, *452*, 301–310.

(115) Miladi, R.; Frikha, N.; Kheiri, A.; Gabsi, S. Energetic Performance Analysis of Seawater Desalination with a Solar Membrane Distillation. *Energy Convers. Manag.* **2019**, *185*, 143–154. https://doi.org/10.1016/j.enconman.2019.02.011.

(116) Avlonitis, S. A.; Kouroumbas, K.; Vlachakis, N. Energy Consumption and Membrane Replacement Cost for Seawater RO Desalination Plants. *Desalination* **2003**, *157* (1–3), 151–158. https://doi.org/10.1016/S0011-9164(03)00395-3.

(117) Zhang, Y.; Peng, Y.; Ji, S.; Li, Z.; Chen, P. Review of Thermal Efficiency and Heat Recycling in Membrane Distillation Processes. *Desalination* **2015**, *367*, 223–239. https://doi.org/10.1016/j.desal.2015.04.013.

(118) Najafi, F.; Alsaffar, M.; Schwerer, S.; Brown, N.; Ouedraogo, J. Environmental Impact Cost Analysis of Multi-Stage Flash, Multi-Effect Distillation, Mechanical Vapor Compression, and Reverse Osmosis Medium-Size Desalination Facilities. In *2016 ASEE Annual Conference & Exposition Proceedings*; ASEE Conferences: New Orleans, Louisiana, 2016; p 26729. https://doi.org/10.18260/p.26729.

(119) Ullah, R.; Khraisheh, M.; Esteves, R. J.; McLeskey, J. T.; AlGhouti, M.; Gad-el-Hak, M.; Vahedi Tafreshi, H. Energy Efficiency of Direct Contact Membrane Distillation. *Desalination* **2018**, *433*, 56–67. https://doi.org/10.1016/j.desal.2018.01.025.

(120) Gude, V. G.; Nirmalakhandan, N. Sustainable Desalination Using Solar Energy. *Energy Convers. Manag.* **2010**, *51* (11), 2245–2251. https://doi.org/10.1016/j.enconman.2010.03.019.

(121) Christie, K. S. S.; Yin, Y.; Lin, S.; Tong, T. Distinct Behaviors between Gypsum and Silica Scaling in Membrane Distillation. *Environ. Sci. Technol.* **2019**, acs.est.9b06023. https://doi.org/10.1021/acs.est.9b06023.

Appendix A: Tabulated Data

Table A1: Feed solutions

Feed	Target Concentration	Target mass (g)	Actual mass (g)	Actual concentration
Na_2SeO_4	500 ppm as SeO_4	0.13215	0.1321	499.8 ppm as SeO_4
Na_2SeO_3	500 ppm as SeO_3	0.13621	0.1362	500 ppm as SeO_3
NaCl	4.0 M	46.752	46.7539	4.0 M
NaCl	1.0 M	11.688 g	11.6875 g	1.0
NaCl	3.5 w/w%	7.0 g	7.0236 g	3.51 wt %
Synthetic FGD	20 g/L as Cl	6.59 g	6.5848 g	19.97 g/L Cl
	500 ppm as SeO4	0.13215 g	0.1321 g	499.8 ppm SeO4

Table A2: Decanoic Acid Mass

Study	Actual DA mass (g)		
	Trial 1	**Trial 2**	**Trial 3**
500 ppm SeO_4	10.0519	10.0627	10.0885
500 ppm SeO_3	10.0516	10.0226	10.0270
4.0 M NaCl	10.0382	10.0022	10.0318
1.0 M NaCl	10.0770	10.0255	10.0427

3.5 wt % NaCl	10.0253	10.0120	10.0009
Synthetic FGD	10.0971	10.0351	10.0477

Table A3: Experimental Data for DA with 4.0 M NaCl feed

Run	Cycle	V_0 mL	V_R mL	Total Rec%	Trial rec %	C_0 M	Cond mS/cm	Cal Curve M	C_F M	Rej%
1	1	10	0.0614	0.00614	0.00614	4	0.01303	5.41E-05	0.044087	98.89783
2	1	10	0.0318	0.00318	0.00318	4	0.007485	2.94E-05	0.046182	98.84544
3	1	10	0.0222	0.00222	0.00222	4	0.004847	1.82E-05	0.040961	98.97596
1	2	9.9386	0.013	0.0013	0.001308	4	0.00257	9.03E-06	0.034741	99.13149
2	2	9.9682	0	0	0	4	NA	NA	NA	NA
3	2	9.9778	0.0309	0.00309	0.003097	4	0.003705	1.35E-05	0.02188	99.45299
1	3	9.9256	0.0296	0.00296	0.002982	4	0.007374	2.89E-05	0.048804	98.7799
2	3	9.9682	0.046	0.0046	0.004615	4	0.006493	2.51E-05	0.027292	99.3177
3	3	9.9469	0.0671	0.00671	0.006746	4	0.02135	9.33E-05	0.069554	98.26116

Table A4: Experimental DATA for DA with 1.0 M NaCl feed

Run	Cycle	V_0 mL	V_R mL	Total Rec%	Trial rec %	C_0 M	Cond mS/cm	Cal Curve M	C_F M	Rej%
1	1	10	0.0251	0.00251	0.00251	1	0.004188	1.55E-05	0.030835	96.91649
2	1	10	0.0603	0.00603	0.00603	1	0.002801	9.93E-06	0.008236	99.17644
3	1	10	0.066	0.0066	0.0066	1	0.00506	1.91E-05	0.014447	98.55527
1	2	9.9749	0	0	0	1	NA	NA	NA	NA
2	2	9.9397	0.0388	0.003904	0.00388	1	0.00419	1.55E-05	0.019958	98.00421
3	2	9.934	0.0323	0.003251	0.00323	1	0.002945	1.05E-05	0.016249	98.37509
1	3	9.9749	0.0507	0.005083	0.00507	1	0.008112	3.21E-05	0.031654	96.83456
2	3	9.9009	0.0419	0.004232	0.00419	1	0.001248	4.07E-06	0.004859	99.51415
3	3	9.9017	0.0485	0.004898	0.00485	1	0.001856	6.31E-06	0.006503	99.34971

Table A5: Experimental Data for DA with 3.5 w/w% NaCl feed

Run	Cycle	V_0 mL	V_R mL	Total Rec%	Trial rec %	C_0 M	Cond mS/cm	Cal Curve M	C_F M	Rej%
1	1	10	0.0314	0.00314	0.00314	0.6	0.002418	8.45E-06	0.013448	97.75874

2	1	10	0.0668	0.00668	0.00668	0.6	0.003683	1.34E-05	0.010055	98.32416
3	1	10	0.0691	0.00691	0.00691	0.6	0.002965	1.06E-05	0.007652	98.72461
1	2	9.9686	0.0271	0.002719	0.00271	0.6	0.001619	5.43E-06	0.01001	98.33167
2	2	9.9332	0.0469	0.004722	0.00469	0.6	0.003081	1.1E-05	0.011762	98.03964
3	2	9.9309	0.0112	0.001128	0.00112	0.6	0.000512	1.52E-06	0.006802	98.86627
1	3	9.9415	0.0507	0.0051	0.00507	0.6	0.002124	7.32E-06	0.007219	98.79688
2	3	9.8863	0.0606	0.00613	0.00606	0.6	0.001175	3.81E-06	0.003143	99.47614
3	3	9.9197	0	0	0	0.6	NA	NA	NA	NA

Table A6: Experimental Data for DPA with 4.0 M NaCl feed

Run	Cycle	V_0 mL	V_R mL	Total Rec%	Trial rec %	C_0 M	Cond mS/cm	Cal Curve M	C_F M	Rej%
1	1	10	1.5884	15.88	15.88	4	0.9062	0.001062868	0.033457	99.16357
2	1	8.4116	0.5305	5.31	6.31	4	1.91	0.004881713	0.460105	88.49738
3	1	7.8811	0.8558	8.56	10.86	4	0.8974	0.001041871	0.060871	98.47822
1	2	10	0.2909	2.91	2.91	4	0.9918	0.001278297	0.219714	94.50715
2	2	9.7091	0.2658	2.66	2.74	4	0.964	0.001205339	0.226738	94.33155
3	2	9.4433	0.2593	2.59	2.75	4	1.130	0.001669063	0.32184	91.95399
1	3	10	0.4431	4.43	4.43	4	1.805	0.004348729	0.490716	87.73209
2	3	9.5569	0.2039	2.04	2.13	4	0.9109	0.00107417	0.263406	93.41485
3	3	9.353	0.2042	2.04	2.18	4	0.7458	0.000713665	0.174747	95.63134

Table A7: Experimental Data for DPA with 1.0 M NaCl feed

Run	Cycle	V_0 mL	V_R mL	Total Rec%	Trial rec %	C_0 M	Cond mS/cm	Cal Curve M	C_F M	Rej%
1	1	10	0.8834	8.83	8.83	1	1.149	0.00172695	0.097744	90.22555
2	1	9.1166	1.1051	11.05	12.12	1	1.643	0.003588042	0.16234	83.76599
3	1	8.0115	0.8675	8.68	10.83	1	1.264	0.00209887	0.120972	87.90277
1	2	10	0.8542	8.54	8.54	1	1.336	0.002350606	0.137591	86.24089
2	2	9.1458	0.8185	8.19	8.95	1	1.266	0.002105666	0.12863	87.13704

3	2	8.3273	0.8975	8.98	10.78	1	1.414	0.002639777	0.147063	85.29372
1	3	10	0.9847	9.85	9.85	1	1.539	0.003138992	0.159388	84.06118
2	3	9.0153	0.8349	8.35	9.26	1	1.517	0.003047927	0.182532	81.74675
3	3	8.1804	0.8726	8.73	10.67	1	1.429	0.002697353	0.154558	84.54416

Table A8: Experimental Data for DPA with 3.5 wt % NaCl feed

Run	Cycle	V_0 mL	V_R mL	Total Rec%	Trial rec %	C_0 M	Cond raw mS/cm	Cal Curve M	C_F M	Rej%
1	1	10	1.0675	10.68	10.68	0.6	1.575	0.003290962	0.154143	74.30943
2	1	8.9325	0.7568	7.57	8.47	0.6	1.252	0.00205833	0.135989	77.33517
3	1	8.1757	1.0001	10.00	12.23	0.6	1.31	0.002258021	0.11289	81.18504
1	2	10	1.0874	10.87	10.87	0.6	1.331	0.002332653	0.107258	82.12362
2	2	8.9126	0.8391	8.39	9.41	0.6	0.973	0.00122821	0.073186	87.80231
3	2	8.0735	1.2456	12.46	15.43	0.6	1.364	0.002452439	0.098444	83.59265
1	3	10	0.9569	9.57	9.57	0.6	1.361	0.002441423	0.127569	78.73843
2	3	9.0431	0.9736	9.74	10.77	0.6	1.172	0.001798372	0.092357	84.60719
3	3	8.0695	1.0738	10.74	13.31	0.6	1.302	0.002229916	0.103833	82.69451

Table A9: Dilution Data for DA ICP-MS Measurements

Sample	DA S1C1 Se04	DA S2C1 SeO4	DA S3C1SeO 4	DA S1C2 SeO4	DA S2C2 SeO4	DA S3 C2 SeO4	DA S1C3 SeO4	DA S2C3 SeO4	DA S3C3 SeO4
Estimated Max conc (ppm)	10	10	10	10	10	10	10	10	10
Estimated Starting Vol (mL)	0.107	0.0623	0.1558	0.0926	0.0246	0.0866	0.0451	0.0759	0.0546
Vol Diluent Added	2.030	1.185	2.960	1.760	4.800	6.580	7.035	1.442	1.037
vv switched to He KED									

Sample	DA S1C1 Se03	dA S2C1 SeO3	DA S3C1 SeO3	DA S1C2 SeO3	DA S2C2 SeO3	DA S3 C2 SeO3	DA S1C3 SeO3	DA S2C3 SeO3	DA S3C3 SeO3
Estimated Max conc (ppm)	10	10	10	10	10	10	10	10	10
Estimated Starting Vol (mL)	0.2422	0.1861	0.1912	0.1621	0.134	0.1172	N/A	0.1426	0.1172
Vol Diluent Added	4.600	3.535	3.635	3.080	2.545	2.230	N/A	2.710	2.230

Table A10: Experimental Data for DA with 500 ppm SeO_4 feed

Run	Cycle	V_0 mL	V_R mL	Total Rec %	Trial rec %	C_0 ppb	ICPMS (CPS)	Cal Curve	Dilution V mL	C_F M	Rej%
1	1	10	0.107	1.07	1.07	500000	7871.6	64.56404	2.03	1289.471	99.74211
2	1	10	0.0623	0.623	0.623	500000	16473.5	135.117	1.185	2705.159	99.45897
3	1	10	0.1558	1.558	1.558	500000	204182.8	1674.728	2.96	33492.41	93.30152
1	2	9.893	0.0926	0.926	0.936015	500000	524395.4	4301.144	1.76	86050.74	82.78985
2	2	9.9377	0.0246	0.246	0.247542	500000	2861.6	23.47111	4.8	4603.199	99.07936
3	2	9.8442	0.0866	0.866	0.879706	500000	49466.4	405.7287	6.58	31233.61	93.75328
1	3	9.8004	0.0451	0.451	0.460185	500000	989.9	8.119387	7.035	1274.636	99.74507
2	3	9.9131	0.0759	0.759	0.765654	500000	1013.5	8.313188	1.442	166.2528	99.96675
3	3	9.7576	0.0546	0.546	0.559564	500000	236.5	1.93981	1.037	38.782	99.99224

Table A11: Experimental Data for DPA with 500 ppm SeO_4 feed

Run	Cycle	V_0 mL	V_R mL	Total Rec %	Trial rec %	C_0 M	ICP MS	Cal Cuve	Dilution V	C_F M	V samp	Rej%
1	1	10	1.1864	11.864	11.864	500000	752.4	119.8386	3	359635.8	0.001	28.07285
2	1	10	1.4224	14.224	14.224	500000	769.7	122.5968	3	367912.9	0.001	26.41742

3	1	10	0.973	9.73	9.73	500000	831.6	132.4525	3	397490.1	0.001	20.50199
1	2	8.8136	1.9345	19.345	21.94903	500000	984.3	156.7683	3	470461.6	0.001	5.907675
2	2	8.5776	1.8153	18.153	21.16326	500000	1064.5	169.5561	3	508837.8	0.001	-1.76756
3	2	9.027	1.4207	14.207	15.73834	500000	1310.0	208.6539	3	626170.3	0.001	-25.2341
1	3	6.8791	1.4717	14.717	21.39379	500000	2461.2	392.0173	3	1176444	0.001	-135.289
2	3	6.7623	0	0	0	500000	NA	NA	NA	NA	0.001	NA
3	3	7.6063	0.6251	6.251	8.218188	500000	1306.7	208.1249	3	624582.8	0.001	-24.9166

Table A12: Experimental Data for DA with 500 ppm SeO_3 feed

Run	Cycle	V_0 mL	V_R mL	Total Rec%	Trial rec %	C_0 M	ICPMS	Cal Curve	Diltuion V	C_F M	Rej%
1	1	10	0.2422	2.422	2.422	500000	915.2	145.772	4.6	2914.356	99.41713
2	1	10	0.1861	1.861	1.861	500000	817.2	130.162	3.535	2602.61	99.47948
3	1	10	0.1912	1.912	1.912	500000	885.7	141.0767	3.635	2823.157	99.43537
1	2	9.7578	0.1621	1.621	1.661235	500000	2019.2	321.6111	3.08	6432.421	98.71352
2	2	9.8139	0.134	1.34	1.365441	500000	4466.9	711.4786	2.545	14224.26	97.15515
3	2	9.8088	0.1172	1.172	1.194845	500000	1741.0	277.3043	2.23	5553.657	98.88927
1	3	9.5957	0	0	0	500000	NA	NA	NA	NA	NA
2	3	9.6799	0.1426	1.426	1.473156	500000	1360.8	216.7503	2.71	4335.918	99.13282
3	3	9.6916	0.1172	1.172	1.209295	500000	2374.0	378.1278	2.23	7572.88	98.48542

Table A13: Experimental Data for DPA with 500 ppm SeO_3 feed

Run	Cycle	V_0 mL	V_R mL	Total Rec %	Trial rec %	C_0 M	ICP MS	Cal Cuve	Dilution V	C_F M	V samp	Rej%

1	1	10	1.8893	18.893	18.893	500000	1761.5	280.5707	3	841992.7	0.001	-68.3985
2	1	10	2.0412	20.412	20.412	500000	838.5	133.5569	3	400804.3	0.001	19.83914
3	1	10	1.0275	10.275	10.275	500000	498.9	79.46448	3	238472.9	0.001	52.30542
1	2	8.1107	1.5716	15.716	19.37687	500000	530.9	84.56019	3	253765.1	0.001	49.24698
2	2	7.9588	1.6214	16.214	20.37242	500000	824.4	131.304	3	394043.4	0.001	21.19132
3	2	8.9725	1.5645	15.645	17.43661	500000	829.3	132.09	3	396402.1	0.001	20.71958
1	3	6.5391	1.3695	13.695	20.94325	500000	905.5	144.217	3	432795.2	0.001	13.44097
2	3	6.3374	1.3283	13.283	20.9597	500000	1347.2	214.5797	4	858533.3	0.001	-71.7067
3	3	7.408	1.3628	13.628	18.39633	500000	658.8	104.9278	3	314888.4	0.001	37.02232

Table A14: Experimental Data for DPA with synthetic FGD feed

Run	Cont.	V_0 mL	V_R mL	Total Rec%	Trial rec %	C0	reading	Cal Curve	Dilution V	C_F M	Rej%
1	NaCl	10	1.1985	11.985	11.985	0.56	1.47100	0.002861943		0.119397	78.67913
	Se		1.1985			500000	144.80000	19.35207955	3	58075.59	88.38488
2	NaCl	10	0.9983	9.983	9.983	0.56	1.35100	0.002404885		0.120449	78.49125
	Se		0.9983			500000	263.40000	35.20260879	3	105643	78.87139
3	NaCl	10	0.716	7.16	7.16	0.56	1.45600	0.002802589		0.195712	65.05151
	Se		0.716			500000	99.70000	13.32460173	3	39987.13	92.00257

Table A15: Experimental data for DA with synthetic FGD feed

Run	Cont.	V_0 mL	V_R mL	Total Rec%	Trial rec %	C0	reading	Cal Curve	Dilution V	C_F M	Rej%
1	NaCl	10	0.0268	0.268	0.268	0.56	0.00217	1.16573 E-05		0.021749	96.11631

	Se		0.0268			500000	229.300 00	30.64524 751	1.528	1777. 882	99.64 442
2	NaCl	10	0.0367	0.367	0.367	0.56	0.00434	2.38153 E-05		0.032 446	94.20 609
	Se		0.0367			500000	2087.00 000	278.9212 018	2.092	16178 .19	96.76 436
3	NaCl	10	0.059	0.59	0.59	0.56	0.00454	2.49484 E-05		0.021 143	96.22 452
	Se		0.059			500000	3834.40 000	512.4558 965	3.363	29722 .44	94.05 551

Appendix B: Additional Figures

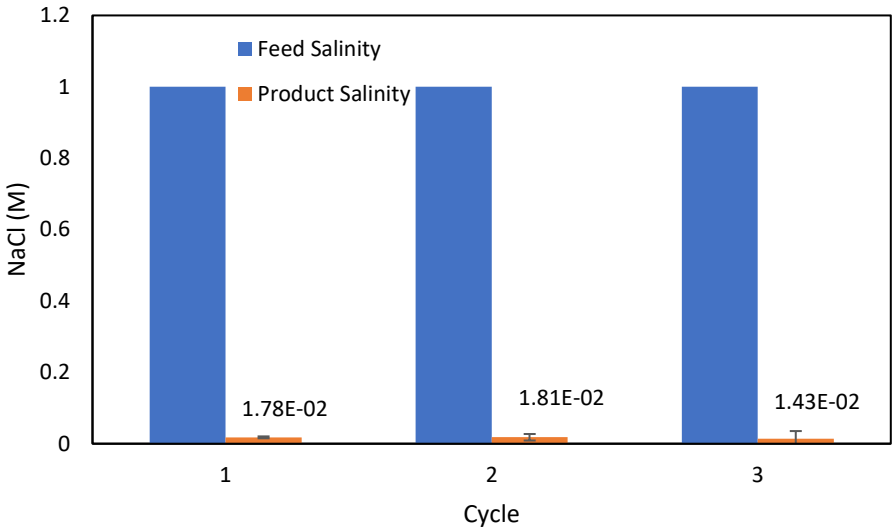

Figure B1: Feed and product water salinity for three cycles of TSSE with 1.0 M NaCl feed and DA solvent.

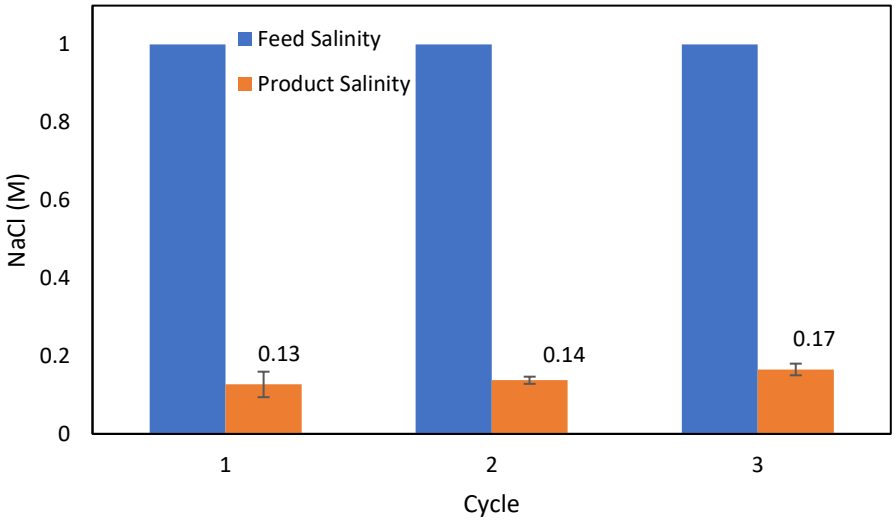

Figure B2: Feed and product water salinity for three cycles of TSSE with 1.0 M NaCl feed and DPA solvent.

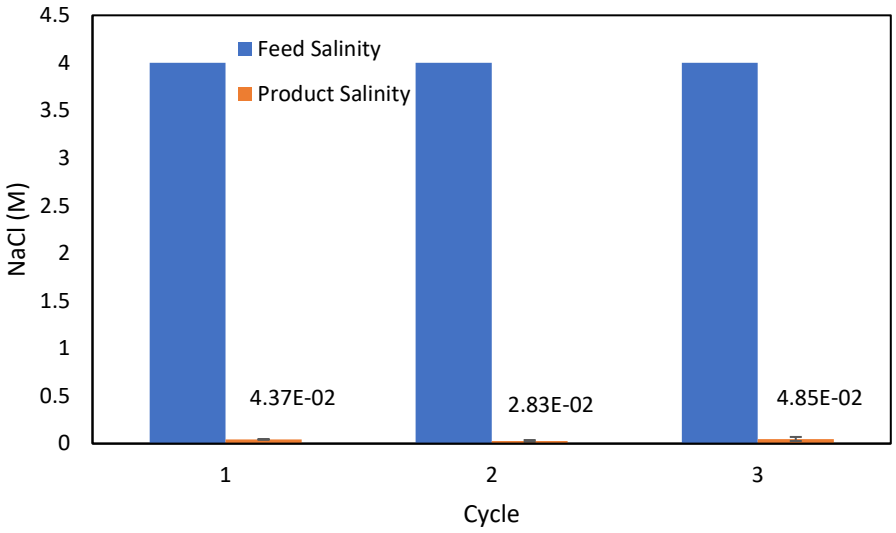

Figure B3: Feed and product water salinity for three cycles of TSSE with 4.0 M NaCl feed and DA solvent.

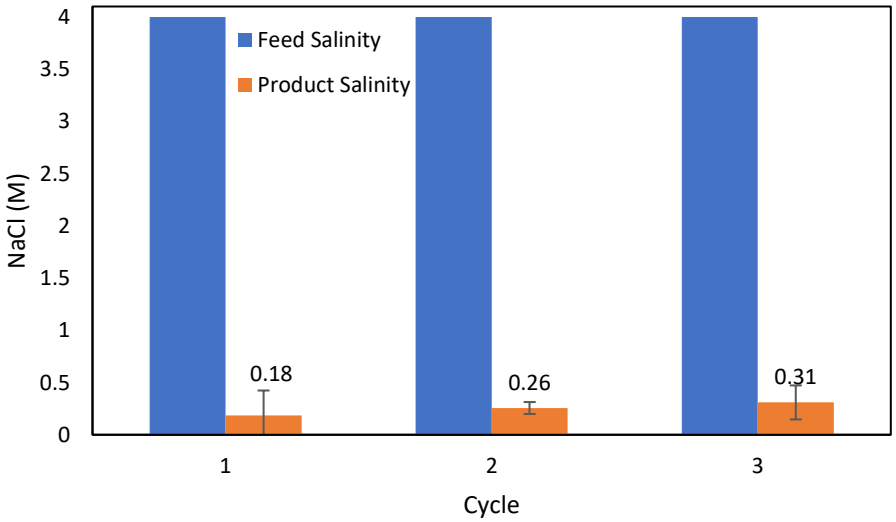

Figure B4: Feed and product water salinity for three cycles of TSSE with 4.0 M NaCl feed and DPA solvent.

Appendix C: Calibration Curves

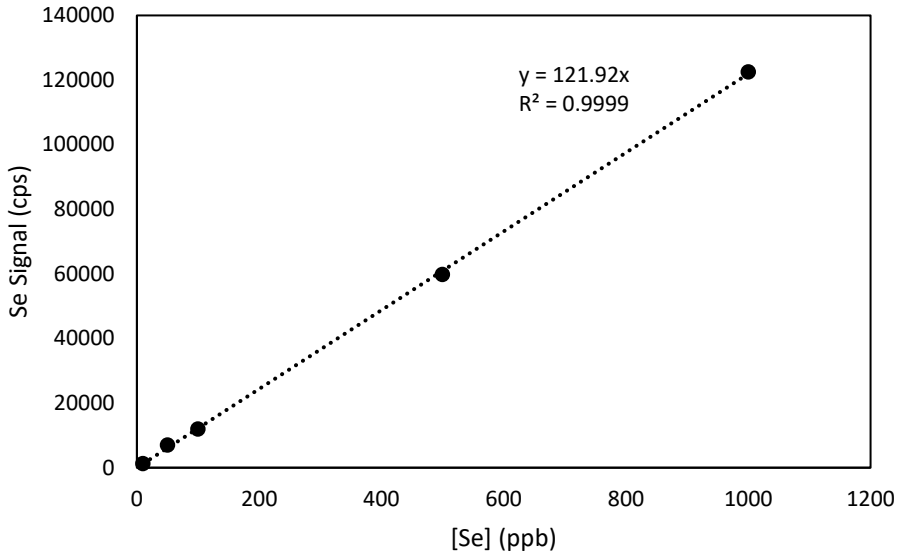

Figure C1: Background-adjusted ICP-MS selenium calibration curve with ammonia collisions. Raw ICP-MS output is counts per second (CPS).

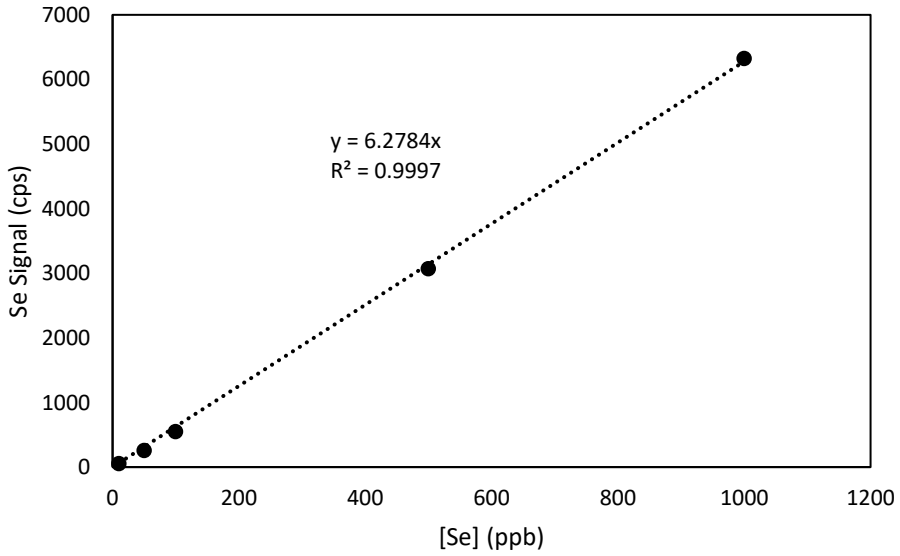

Figure C2: Background-adjusted ICP-MS selenium calibration curve with helium collisions.

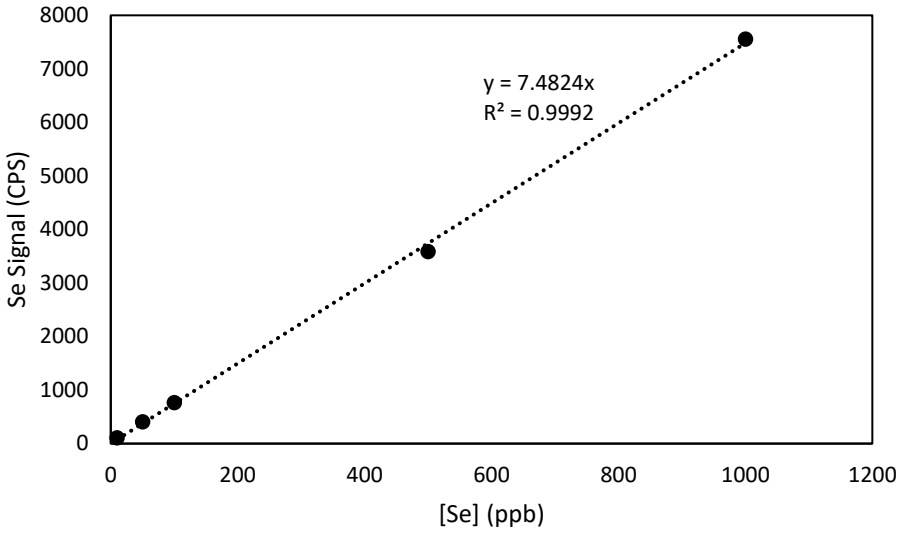

Figure C3: Background-adjusted ICP-MS selenium calibration curve with helium collisions for synthetic FGD measurements.